THE UNIVERSITY of EDINBURGH

Edinburgh Research Explorer

Molecular kinetic modelling of non-equilibrium transport of confined van der Waals fluids

Citation for published version:
Shan, B, Su, W, Gibelli, L & Zhang, Y 2023, 'Molecular kinetic modelling of non-equilibrium transport of confined van der Waals fluids', *Journal of Fluid Mechanics*, vol. 976. https://doi.org/10.1017/jfm.2023.893

Digital Object Identifier (DOI):
10.1017/jfm.2023.893

Link:
Link to publication record in Edinburgh Research Explorer

Document Version:
Peer reviewed version

Published In:
Journal of Fluid Mechanics

General rights
Copyright for the publications made accessible via the Edinburgh Research Explorer is retained by the author(s) and / or other copyright owners and it is a condition of accessing these publications that users recognise and abide by the legal requirements associated with these rights.

Take down policy
The University of Edinburgh has made every reasonable effort to ensure that Edinburgh Research Explorer content complies with UK legislation. If you believe that the public display of this file breaches copyright please contact openaccess@ed.ac.uk providing details, and we will remove access to the work immediately and investigate your claim.

OPEN ACCESS

Download date: 13. Dec. 2023

Banner appropriate to article type will appear here in typeset article

Molecular kinetic modelling of non-equilibrium transport of surface-confined van der Waals fluids

Baochao Shan[1], Wei Su [2,3], Livio Gibelli [1], and Yonghao Zhang[4]†

[1]School of Engineering, University of Edinburgh, Edinburgh EH9 3FB, UK

[2]Division of Emerging Interdisciplinary Areas, The Hong Kong University of Science and Technology, Clear Water Bay, Hong Kong, China

[3]Department of Mathematics, The Hong Kong University of Science and Technology, Clear Water Bay, Hong Kong, China

[4]State Key Laboratory of High Temperature Gas Dynamics, Institute of Mechanics, Chinese Academy of Sciences, Beijing 100190, China

(Received xx; revised xx; accepted xx)

A thermodynamically consistent kinetic model is proposed for non-equilibrium transport of surface-confined van der Waals fluids, where the long-range molecular attraction is considered by a mean-field term in the transport equation and the transport coefficients including shear and bulk viscosities and thermal conductivity are tuned to match the experimental data. Equation of states of van der Waals type can be obtained from appropriate choice of the radial distribution function, while in the modified Enskog theory nonphysical negative transport coefficients appear near the critical temperature and the Boltzmann equation may not be recovered in the dilute limit. The shear viscosity and thermal conductivity are more accurately predicted by taking gas molecular attraction into account, while the *softened* Enskog formula for hard-sphere molecules performs better in predicting the bulk viscosity. The present kinetic model agrees with the Boltzmann model in the dilute limit and with the Navier-Stokes equations in the continuum limit, which indicates its capability in modelling of dilute-to-dense and continuum-to-non-equilibrium flows. The new model is thoroughly examined and validated by comparing with the molecular dynamics simulation results. In contrast to the previous studies, our simulation results reveal the importance of molecular attraction even for high temperatures which holds the molecules to the bulk while the hard-sphere model significantly overestimates the density near the wall. Because the long-range molecular attraction is appropriately considered in the present model, the velocity slip and temperature jump at the surface for realistic van der Waals fluids can be accurately predicted.

Key words:

† Email address for correspondence: yonghao.zhang@imech.ac.cn

Abstract must not spill onto p.2

1. Introduction

The transport of van der Waals fluids through micro-/nano-scale surface-confined geometries appears in many engineering applications, such as shale gas production (Wu *et al.* 2016; Mehrabi *et al.* 2017), carbon dioxide geological sequestration (Wang *et al.* 2018), energy-efficient cooling (Rana *et al.* 2018; Van Erp *et al.* 2020), and ultrafast filtration using membranes (Joseph & Aluru 2008; Torres-Herrera & Poiré 2021). The definition of van der Waals fluids originates from the celebrated van der Waals equation of state (EoS) (van der Waals 1873; Maxwell 1874), which extends the ideal gas law by coupling the effects of both the finite size of gas molecules and the long-range attraction between gas molecules. The EoS for van der Waals fluids is given below,

$$p = \frac{nk_BT}{1 - nV_0} - an^2, \tag{1.1}$$

where p is the pressure, n is the gas number density, T is the temperature, k_B is the Boltzmann constant, $V_0 = 2\pi\sigma^3/3$ is the excluded volume per molecule with σ being the molecular diameter, and a is a constant that measures the average attraction between fluid molecules, which can be determined from the critical pressure and temperature of the fluids.

The gas volume exclusion and long-range molecular attraction are known as the real gas effect (Wang *et al.* 2018; Zhang *et al.* 2019), which plays a prominent role in high-pressure scenarios (Shan *et al.* 2021) or at near-critical regions (Restrepo & Simões-Moreira 2022). In conventional hydrodynamics, the real gas effect is empirically considered by using the realistic EoS with the Euler or Navier-Stokes (NS) equations (Zhao *et al.* 2014; Restrepo & Simões-Moreira 2022), which is valid for equilibrium or near-equilibrium flows. For flows far from equilibrium, these continuum models are no longer applicable (Torrilhon 2016; Rana *et al.* 2018). In addition, surface confinement can lead to inhomogeneities of not only in density but also in transport coefficients (e.g. shear viscosity and thermal conductivity). However, the van der Waals EoS assumes homogeneous fluid density (Maxwell 1874) and the NS equations assume constant transport coefficients in confined spaces (Todd 2001), making the continuum models inadequate to capture inhomogeneous molecular flow features (Kogan 1973).

Consequently, an accurate model of van der Waals fluids under tight surface-confinement requires simultaneous consideration of the effects of real gas, rarefaction, and surface-confinement, which still remains as a research challenge.

At the molecular scale, molecular dynamics (MD) simulations can provide an accurate computational tool for investigating gas dynamics under tight surface-confinement. In MD simulations, the van der Waals interactions are mostly described by 12-6 Lennard-Jones (LJ) potential (Martini *et al.* 2008), i.e.

$$\phi(r) = 4\epsilon\left[\left(\frac{\sigma}{r}\right)^{12} - \left(\frac{\sigma}{r}\right)^{6}\right], \tag{1.2}$$

where ϵ and σ are the characteristic energy and length (equivalently the molecular diameter) scales, respectively, and r is the distance between molecules. The LJ potential is composed of a strong repulsive part and a weak long-range attractive tail, which describes the real gas effect from a molecular perspective and captures the fluid inhomogeneity caused by the confinement. However, MD simulations are prohibitively expensive for most practical simulations (Nie *et al.* 2004; Sheng *et al.* 2020), and suffer from statistical noise for low-speed flows when the flow velocity is significantly smaller than thermal motions of fluid molecules. Consequently, a multiscale model is required to capture both molecular and continuum effects.

Kinetic theory relates the molecular-scale dynamics to the continuum-scale flow properties, serving as a bridge between the continuum and atomistic worlds (Kogan 1973; Guo & Shu 2013; Gan *et al.* 2022). The fundamental equation in kinetic theory is the Boltzmann equation for ideal gases (Takata & Noguchi 2018). However, it becomes invalid in scenarios where the gas molecule size is comparable to (i) the gas mean free path (e.g. dense gas flows) (Cercignani & Lampis 1988; Sadr & Gorji 2017; Wang *et al.* 2020) or (ii) the characteristic length of the flow domain (e.g. nano-confined flows) (Shan *et al.* 2020; Sheng *et al.* 2020; Corral-Casas *et al.* 2022).

Enskog (1921) extended the localised Boltzmann collision operator to a non-localised one by considering the finite size of gas molecules, so that the instantaneous collisional transfer of momentum and energy over a molecule size comes into play (Frezzotti 1999). The finite size of gas molecules will increase the collision frequency by reducing the free streaming space for gas molecules by a factor of $(1-2nV_0)$ and decrease the collision frequency by shielding other molecules (Chapman & Cowling 1990; Wang & Li 2007) by a factor of $(1-11nV_0/8)$, so that the overall change in collision frequency is quantified by the radial distribution function χ, i.e.

$$\chi^{Enskog} = \frac{1-\frac{11}{8}nV_0}{1-2nV_0}. \tag{1.3}$$

The Standard Enskog Theory (SET) was refined by van Beijeren & Ernst (1973) to guarantee the irreversible thermodynamics for dense gas mixtures of hard-sphere molecules and yield the correct single-particle equilibrium distribution function (van Beijeren 1983), which is now known as the Revised Enskog Theory (RET). Both SET and RET for dense gases have been rather successful in predicting transport properties of simple fluids (Hanley *et al.* 1972; Amorós *et al.* 1992), shock waves propagation (Frezzotti 1997), and gas dynamics under confinement (Wu *et al.* 2016; Sheng *et al.* 2020). However, SET and RET ignore the long-range attractive interactions between gas molecules, which are important in real gases (Vera & Prausnitz 1972; He & Doolen 2002; Wang & Li 2007; Frezzotti *et al.* 2019).

Two approaches have been developed to describe the dynamics of van der Waals fluids, namely the Modified Enskog Theory (MET) (Chapman & Cowling 1990; Amorós *et al.* 1992; Luo 2000) and the mean-field approximation (Sobrino 1967; Karkheck & Stell 1981). MET imposes two modifications to the radial distribution function and the covolume for more realistic molecular interactions. One is to use the thermal pressure $T(\partial p/\partial T)_V$ from experimental data (Hanley *et al.* 1972; Amorós *et al.* 1992) or the van der Waals pressure (i.e. the pressure in the van der Waals-type EoS) (Luo 2000) to replace the pressure p^{hs} in the hard-sphere EoS $p^{hs} = nk_BT(1+nV_0\chi)$. With (1.1), the radial distribution function becomes

$$\chi^{MET} = \frac{1}{1-nV_0} - \frac{a}{k_BTV_0}, \tag{1.4}$$

where both the volume exclusion and the molecular attraction are taken into account. The other modification is to correct the covolume V_0 according to either the second virial coefficient (Hanley *et al.* 1972; Amorós *et al.* 1992) or the experimental data of the transport coefficients (Chapman & Cowling 1990). However, the MET has only been applied to obtain transport coefficients of dense real gases, while no application to gas dynamics has been reported. In addition, the MET can result in a negative radial distribution function, and thus negative transport coefficients for real gases, which is not physical.

The mean-field approximation adds a weak attractive tail to the Enskog equation to account for the long-range molecular attraction (Sobrino 1967), resulting the Enskog-Vlasov (EV) equation (Karkheck & Stell 1981; Sadr *et al.* 2021). Furthermore, a state-dependent hard-sphere diameter, as commonly discussed in perturbation theories for classical fluids (Barker

& Henderson 1967; Andersen *et al.* 1971; Cotterman *et al.* 1986), can be chosen for a better approximation of real fluids (Karkheck & Stell 1981; Guo *et al.* 2006). In this way, the hard-core repulsion is *softened* to account for the softness of the repulsive potential (Ben-Amotz & Herschbach 1990), which modifies the transport coefficients. However, the EV collision operator still considers hard-sphere molecules. A more realistic molecular potential model (e.g. LJ type) needs to be considered for molecular collisions.

Although the van der Waals-type EoS can be recovered, both the MET and the EV equation have their own problems in modelling van der Waals fluids, e.g. recovering correct transport coefficients. Therefore, it is still an open question about how to model molecular attraction in the kinetic theory of dense gases (Luo 1998; He *et al.* 1998; Luo 2000; He & Doolen 2002). Another major issue that hinders the application of kinetic models is its computational complexity and cost. As the computational cost of solving the Enskog and EV equations directly using either probabilistic or deterministic method is prohibitive (Frezzotti & Sgarra 1993; Alexander *et al.* 1995; Sadr & Gorji 2019; Frezzotti *et al.* 2019; Wu *et al.* 2015, 2016), simplified models have been proposed to achieve efficient computations using the relaxation time approach, e.g.(Luo 1998; He *et al.* 1998; Wang *et al.* 2020; Su *et al.* 2023). Based on the intuitive observations of the underlying molecular physics, various types of simple kinetic models (Suryanarayanan *et al.* 2013; Takata & Noguchi 2018; Takata *et al.* 2021) have been developed for the van der Waals fluids, which have been successfully applied to the study of phase transition problems. However, these models are either limited to the low-speed/isothermal flows or fail to reproduce the correct transport coefficients. In this study, we will therefore review the available approaches theoretically and numerically, and attempt to develop an improved kinetic model for the van der Waals fluids that is computationally efficient to solve.

To develop an efficient and accurate kinetic model to describe surface-confined non-equilibrium transport of van der Waals fluids, the following considerations are made:

(i) the volume exclusion is described for both hard-sphere and LJ molecular interactions, with appropriate modifications of the transport coefficients, so that the kinetic model is not only mathematically simpler than the Enskog and EV equations, but also physically more appropriate;

(ii) the long-range molecular attraction is considered in a thermodynamically consistent manner;

(iii) the kinetic model reduces to the Boltzmann model equation in the dilute gas limit, i.e. when $\chi \rightarrow 1$ and $\sigma \rightarrow 0$;

(iv) it recovers the NS equations in the continuum limit, i.e. when $H/\sigma \rightarrow \infty$ and $\mathrm{Kn} \rightarrow 0$;

(v) the non-equilibrium (e.g. velocity slip), thermal (e.g. temperature jump), and confinement (e.g. inhomogeneous fluid properties) effects can be accurately captured.

The remainder of the paper is organised as follows: in §2, a simplified kinetic model for van der Waals fluids is developed starting from the generalised Boltzmann equation using the mean-field approximation. Through the Chapman-Enskog expansion, we show that the correct EoS can be recovered from the kinetic model to achieve thermodynamic consistency, where the relaxation time and Prandtl number (Pr) can be determined using the transport coefficients of real gases. In §3, numerical simulations are performed to validate the model and to understand the effects of long-range molecular attraction and viscous dissipation on gas dynamics at different density, non-equilibrium and confinement conditions, using the MD data serves as a benchmark. We also show that the current kinetic model reduces to the Shakhov model for hard-sphere molecules in the dilute limit and recovers the NS equations when the confinement and non-equilibrium effects are negligible. Finally, the conclusions are drawn in §4.

Focus on Fluids articles must not exceed this page length

2. Kinetic modelling of van der Waals fluids

As the gas density increases, the assumptions of binary collisions and molecular chaos that underlie the Boltzmann equation become inappropriate. For dense gases, the molecular interactions, including short-range repulsion and long-range attraction, play a prominent role, especially in applications such as phase transitions (Frezzotti *et al.* 2019; Huang *et al.* 2021) and multiphase flows (Sadr *et al.* 2021; Huang *et al.* 2022). A rigorous description of dense gases is the generalised Boltzmann equation derived from the Liouville equation (Ferziger & Kaper 1972; He & Doolen 2002), in which the evolution of the one-particle distribution function can be written as

$$\frac{\partial f}{\partial t} + \boldsymbol{\xi} \cdot \nabla f + \frac{\boldsymbol{F}_{ext}}{m} \cdot \nabla_{\xi} f = \iint \frac{\partial f^{(2)}}{\partial \boldsymbol{\xi}} \cdot \nabla \phi(\boldsymbol{r}, \boldsymbol{r}_1) \mathrm{d}\boldsymbol{\xi}_1 \mathrm{d}\boldsymbol{r}_1, \tag{2.1}$$

where $f = f(\boldsymbol{r}, \boldsymbol{\xi}, t)$ is the velocity distribution function of molecular velocity $\boldsymbol{\xi}$ at the spatial position $\boldsymbol{r}$ and the time t; $\boldsymbol{F}_{ext}$ is the external force; $f^{(2)} = f(\boldsymbol{r}, \boldsymbol{\xi}, \boldsymbol{r}_1, \boldsymbol{\xi}_1, t)$ is the two-particle distribution function, and $\phi(\boldsymbol{r}, \boldsymbol{r}_1)$ is the pairwise intermolecular potential. For the LJ potential (1.2), it can be decomposed into a short-range repulsive core ϕ_{rep} and a long-range attractive tail ϕ_{att} according to perturbation rules (Barker & Henderson 1967; Andersen *et al.* 1971; Cotterman *et al.* 1986). Furthermore, two simplifications are made on the two-particle distribution function. First, fluid molecules are assumed to satisfy the molecular chaos hypothesis, i.e. the velocities of colliding molecules are not correlated and independent of the position so that the two-particle distribution function can be expressed by the product of two one-particle distribution functions, i.e.

$$f(\boldsymbol{r}, \boldsymbol{\xi}, \boldsymbol{r}_1, \boldsymbol{\xi}_1, t) = \chi\left(\frac{\boldsymbol{r} + \boldsymbol{r}_1}{2}\right) f(\boldsymbol{r}, \boldsymbol{\xi}, t) f(\boldsymbol{r}_1, \boldsymbol{\xi}_1, t). \tag{2.2}$$

The second simplification is based on the observation that the radial distribution function is approximately unity in the attractive range (Reichl 1998). With these two simplifications, the generalised Boltzmann equation can be transformed to

$$\frac{\partial f}{\partial t} + \boldsymbol{\xi} \cdot \nabla f + \frac{\boldsymbol{F}_{ext} + \boldsymbol{F}_{att}}{m} \cdot \nabla_{\xi} f = J_E, \tag{2.3}$$

where J_E and $\boldsymbol{F}_{att}$ are the Enskog collision operator and the mean-field force for molecular attractions, respectively. Equation (2.3) is also known as the EV equation (Sobrino 1967). The Enskog collision operator can be expressed as

$$J_E(f, f) = \sigma^2 \iint \begin{bmatrix} \chi(\boldsymbol{r} + \frac{1}{2}\sigma\boldsymbol{k}) f(\boldsymbol{r}, \boldsymbol{\xi}') f_1(\boldsymbol{r} + \sigma\boldsymbol{k}, \boldsymbol{\xi}_1') \\ -\chi(\boldsymbol{r} - \frac{1}{2}\sigma\boldsymbol{k}) f(\boldsymbol{r}, \boldsymbol{\xi}) f_1(\boldsymbol{r} - \sigma\boldsymbol{k}, \boldsymbol{\xi}_1) \end{bmatrix} \boldsymbol{g} \cdot \boldsymbol{k} \mathrm{d}\boldsymbol{k} \mathrm{d}\boldsymbol{\xi}_1, \tag{2.4}$$

where $\boldsymbol{g} = \boldsymbol{\xi}_1 - \boldsymbol{\xi}$ is the relative velocity of two colliding molecules, $\boldsymbol{k} = (\boldsymbol{r}_1 - \boldsymbol{r})/|\boldsymbol{r}_1 - \boldsymbol{r}|$ is the unit vector that specifies the relative position of two colliding molecules, and $\boldsymbol{\xi}'$ and $\boldsymbol{\xi}_1'$ are the post-collision velocities, which are related to the pre-collision velocities $\boldsymbol{\xi}$ and $\boldsymbol{\xi}_1$ through

$$\boldsymbol{\xi}' = \boldsymbol{\xi} + \boldsymbol{k}(\boldsymbol{g} \cdot \boldsymbol{k}), \quad \boldsymbol{\xi}_1' = \boldsymbol{\xi}_1 - \boldsymbol{k}(\boldsymbol{g} \cdot \boldsymbol{k}). \tag{2.5}$$

Meanwhile, the mean-field force term can be expressed as

$$\boldsymbol{F}_{att} = -\nabla \left[\int_{|\boldsymbol{r}'| > \sigma} n(\boldsymbol{r}_1) \phi_{att}(\boldsymbol{r}, \boldsymbol{r}_1) \mathrm{d}\boldsymbol{r}_1 \right]. \tag{2.6}$$

To better represent realistic gases, the hard-sphere collisions (2.4) are *softened* by taking a state-dependent molecular diameter according to the perturbation theories (Barker & Henderson 1967; Andersen *et al.* 1971; Cotterman *et al.* 1986). For example, the effective molecular diameter, according to Barker & Henderson (1967), can be calculated as

$$\sigma_e = \sigma \int_0^{\infty} \left\{ 1 - \exp\left[-\frac{\phi(r)}{k_B T} \right] \right\} \mathrm{d}r, \tag{2.7}$$

which decreases with increasing temperature and plays a role similar to that of two colliding molecules penetrating into each other. It is not surprising that this state-dependent molecular diameter changes the transport coefficients. Shear viscosity μ_s^{hs} and thermal conductivity κ^{hs} can be calculated as

$$\mu_s^{hs} = \frac{1}{\chi}[1 + 0.8 n V_0 \chi + 0.7614 (n V_0 \chi)^2] \mu_0, \tag{2.8}$$

and

$$\kappa^{hs} = \frac{1}{\chi}[1 + 1.2 n V_0 \chi + 0.7574 (n V_0 \chi)^2] \kappa_0, \tag{2.9}$$

respectively, with μ_0 and κ_0 being the viscosity and thermal conductivity at the atmospheric pressure, respectively. Although a state-dependent diameter aims for a better approximation of the molecular collision process, the Enskog collision operator (2.4) is still for hard-sphere gases. Ideally, more general molecular interaction models such as the LJ potential should be considered in the collision operator.

Equation (2.3) combined with (2.4) and (2.6) formulates an integral procedure to simulate the dynamics of van der Waals fluids. However, the collision operator (2.4) is more complex than the Boltzmann collision operator, so a simplified model is required to achieve computational efficiency with reasonable simulation accuracy.

2.1. *The simplified kinetic model for van der Waals fluids*

Following our previous works (Wang *et al.* 2020; Su *et al.* 2023), we expand the collision operator (2.4) into a Taylor series near $\boldsymbol{r}$ and retain up to the second order terms as shown below,

$$J_E(f,f) = \chi J^{(0)}(f,f) + J^{(1)}(f,f) + J^{(2)}(f,f), \tag{2.10}$$

with

$$\begin{aligned}
J^{(0)}(f,f) &= \sigma^2 \iint (f' f_1' - f f_1) \boldsymbol{g} \cdot \boldsymbol{k} \mathrm{d}\boldsymbol{k} \mathrm{d}\boldsymbol{\xi}_1, \\
J^{(1)}(f,f) &= \sigma^3 \chi \iint \boldsymbol{k} \cdot (f' \nabla f_1' + f \nabla f_1) \boldsymbol{g} \cdot \boldsymbol{k} \mathrm{d}\boldsymbol{k} \mathrm{d}\boldsymbol{\xi}_1 \\
&\quad + \frac{\sigma^3}{2} \iint \boldsymbol{k} \cdot \nabla \chi (f' f_1' + f f_1) \boldsymbol{g} \cdot \boldsymbol{k} \mathrm{d}\boldsymbol{k} \mathrm{d}\boldsymbol{\xi}_1, \\
J^{(2)}(f,f) &= \frac{\sigma^4}{2} \chi \iint \boldsymbol{k}\boldsymbol{k} : (f' \nabla\nabla f_1' - f \nabla\nabla f_1) \boldsymbol{g} \cdot \boldsymbol{k} \mathrm{d}\boldsymbol{k} \mathrm{d}\boldsymbol{\xi}_1 \\
&\quad + \frac{\sigma^4}{2} \iint \boldsymbol{k} \cdot \nabla \chi [\boldsymbol{k} \cdot (f' \nabla f_1' - f \nabla f_1)] \boldsymbol{g} \cdot \boldsymbol{k} \mathrm{d}\boldsymbol{k} \mathrm{d}\boldsymbol{\xi}_1 \\
&\quad + \frac{\sigma^4}{8} \iint \boldsymbol{k}\boldsymbol{k} : \nabla\nabla \chi (f' f_1' - f f_1)] \boldsymbol{g} \cdot \boldsymbol{k} \mathrm{d}\boldsymbol{k} \mathrm{d}\boldsymbol{\xi}_1
\end{aligned} \tag{2.11}$$

where all the quantities are evaluated at the position $\boldsymbol{r}$, and $J^{(0)}(f,f)$ is the Boltzmann collision operator for dilute gases, which can be further simplified by kinetic models. Here, we choose the Shakhov model (Shakhov 1968), which is written as

$$J^{(0)}(f,f) \equiv J_s = -\frac{1}{\tau_s}\left[(f-f^{eq}) - f^{eq}(1-\mathrm{Pr})\frac{\boldsymbol{\xi}\cdot\boldsymbol{Q}_k}{5p_0RT}\left(\frac{\xi^2}{RT}-5\right)\right], \tag{2.12}$$

where τ_s is the relaxation time, Pr is the Prandtl number, $\boldsymbol{Q}_k$ is the heat flux due to the translational motion of gas molecules, $\boldsymbol{c} = \boldsymbol{\xi} - \boldsymbol{u}$ is the peculiar velocity, $p_0 = nk_BT$ is the EoS for ideal gases, $R = k_B/m$ is the specific gas constant, and f^{eq} is the Maxwellian distribution function, which reads as

$$f^{eq} = n\left(\frac{m}{2\pi k_BT}\right)^{\frac{3}{2}}\exp\left(-\frac{mc^2}{2k_BT}\right). \tag{2.13}$$

The terms $J^{(1)}(f,f)$ and $J^{(2)}(f,f)$ describe the dense gas effect arising from increasing density. Considering that (i) for dilute gases far from equilibrium, the density terms $J^{(1)}(f,f)$ and $J^{(2)}(f,f)$ are negligible and the non-equilibrium effect can be captured by the Shakhov model (2.12); (ii) for gases at high densities, the density terms $J^{(1)}(f,f)$ and $J^{(2)}(f,f)$ become important, where the gas mean free path should be small as $\lambda \propto 1/n$, implying that the gases are not far from equilibrium; and (iii) for gases not far from equilibrium, the equilibrium distribution function f^{eq} is the leading part of the distribution function f, further simplifications can be made on $J^{(1)}(f,f)$ and $J^{(2)}(f,f)$ by replacing the velocity distribution functions therein with their corresponding equilibrium distribution functions, leading to the following two terms as (Rangel-Huerta & Velasco 1996; Kremer 2010; Wang *et al.* 2020; Su *et al.* 2023)

$$J^{(1)}(f,f) \equiv \mathcal{I}^{(1)} = -nV_0\chi f^{eq}\left\{\begin{aligned}&\boldsymbol{c}\cdot\left[\nabla\ln(n^2\chi T) + \frac{3}{5}\left(C^2-\frac{5}{2}\right)\nabla\ln T\right]\\ &+\frac{2}{5}\left[2\boldsymbol{C}\boldsymbol{C}:\nabla\boldsymbol{u} + \left(C^2-\frac{5}{2}\right)\nabla\cdot\boldsymbol{u}\right]\end{aligned}\right\}, \tag{2.14}$$

and

$$J^{(2)}(f,f) \equiv \mathcal{I}^{(2)} = \nabla\cdot\left[f^{eq}\frac{\mu_B}{p_0}(\nabla\cdot\boldsymbol{u})\left(C^2-\frac{3}{2}\right)\boldsymbol{c}\right] + \mathcal{R}, \tag{2.15}$$

where $\boldsymbol{C} = (m/2k_BT)^{1/2}\boldsymbol{c}$ is the non-dimensional peculiar velocity, μ_B is the bulk viscosity. $\mathcal{R}$ is a second order quantity which has no contribution to the transfer of mass, momentum and energy, so it can be ignored hereafter in the kinetic model.

It should be noted that the bulk viscosity μ_B appears in the expansion of the Enskog equation, but is absent in previous kinetic models (Luo 1998; He & Doolen 2002; Wang *et al.* 2020; Takata *et al.* 2021). Although it is a small quantity involved in the second order term of the Taylor series (Rangel-Huerta & Velasco 1996; Kremer 2010), it is important in many applications (Jaeger *et al.* 2018), such as sound attenuation and shock wave propagation, where gases undergo strong compression or expansion (Hoover *et al.* 1980*a*,*b*).

For simplicity, the radial distribution function χ in (2.10) can be absorbed into the relaxation time τ_s in (2.12). The final evolution equation of the kinetic model for van der Waals fluids can be written as

$$\frac{\partial f}{\partial t} + \boldsymbol{\xi}\cdot\nabla f + \frac{\boldsymbol{F}_{ext}+\boldsymbol{F}_{att}}{m}\cdot\nabla_{\xi} f = J_s^{(0)} + \mathcal{I}^{(1)} + \mathcal{I}^{(2)}, \tag{2.16}$$

where

$$J_s^{(0)} = -\frac{1}{\tau}\left[(f-f^{eq}) - f^{eq}(1-\mathrm{Pr})\frac{\boldsymbol{\xi}\cdot\boldsymbol{Q}_k}{5p_0RT}\left(\frac{\xi^2}{RT}-5\right)\right], \tag{2.17}$$

with the relaxation time $\tau = \tau_s/\chi$. The attractive part of the LJ potential, i.e., $\phi_{att} = -4\epsilon(\sigma/r)^6$ is chosen to simulate the molecular attraction in the mean-field force term (2.6). It should be emphasised that equation (2.16) is accurate to the second order in the Taylor series of the Enskog collision operator (2.4) with omitted second order quantities which have no contribution to mass, momentum and energy transfer. The macroscopic properties can then be obtained by taking moments of the distribution function, i.e.

$$n(\boldsymbol{r},t) = \int f(\boldsymbol{r},\boldsymbol{\xi},t)\mathrm{d}\boldsymbol{\xi}, \tag{2.18a}$$

$$n\boldsymbol{u}(\boldsymbol{r},t) = \int \boldsymbol{\xi} f(\boldsymbol{r},\boldsymbol{\xi},t)\mathrm{d}\boldsymbol{\xi}, \tag{2.18b}$$

$$\frac{3}{2}nk_BT(\boldsymbol{r},t) = \int \frac{m}{2}c^2 f(\boldsymbol{r},\boldsymbol{\xi},t)\mathrm{d}\boldsymbol{\xi}, \tag{2.18c}$$

$$\boldsymbol{P}_k(\boldsymbol{r},t) = \int m\boldsymbol{c}\boldsymbol{c} f(\boldsymbol{r},\boldsymbol{\xi},t)\mathrm{d}\boldsymbol{\xi}, \tag{2.18d}$$

$$\boldsymbol{Q}_k(\boldsymbol{r},t) = \int \frac{m}{2}c^2\boldsymbol{c} f(\boldsymbol{r},\boldsymbol{\xi},t)\mathrm{d}\boldsymbol{\xi}, \tag{2.18e}$$

where $\boldsymbol{P}_k$ and $\boldsymbol{Q}_k$ are the kinetic stress tensor and heat flux, respectively, which arise from the free streaming of gas molecules.

It should be noted that although the collisional terms $J_s^{(0)}$, $\mathcal{I}_1$ and $\mathcal{I}_2$ are derived from the Enskog collision operator (2.4), the kinetic model (2.16) is not restricted to hard-sphere molecules as the transport coefficients are corrected to account for the influence of inter-molecular potentials. In the following sections, we will demonstrate the thermodynamic consistency of our kinetic model and how to obtain correct transport coefficients.

2.2. *The hydrodynamic equations and relaxation time*

Using the Chapman-Enskog expansion (see Appendix A for the details), the following hydrodynamic equations can be obtained

$$\begin{aligned}
&\frac{\partial \rho}{\partial t} + \nabla\cdot(\rho\boldsymbol{u}) = 0,\\
&\frac{\partial(\rho\boldsymbol{u})}{\partial t} + \nabla\cdot(\rho\boldsymbol{u}\boldsymbol{u}) + \nabla[p-\mu_B(\nabla\cdot\boldsymbol{u})] - \nabla\cdot(2\mu_s\mathring{\boldsymbol{S}}) - \nabla\cdot\boldsymbol{K} - n\boldsymbol{F}_{ext} = 0,\\
&\frac{\partial(\rho E)}{\partial t} + \nabla\cdot(\rho E\boldsymbol{u}) - \nabla\cdot(\kappa\nabla T) + [p-\mu_B(\nabla\cdot\boldsymbol{u})](\nabla\cdot\boldsymbol{u}) - (2\mu_s\mathring{\boldsymbol{S}}):\nabla\boldsymbol{u}\\
&\qquad -\boldsymbol{K}:\nabla\boldsymbol{u} - n\boldsymbol{F}_{ext}\cdot\boldsymbol{u} = 0,
\end{aligned} \tag{2.19}$$

where the shear viscosity μ_s and thermal conductivity κ relate to the relaxation time τ and the Prandtl number Pr through (A 13). Accordingly, the relaxation time τ and the Prandtl number Pr can be obtained as

$$\begin{aligned}
\tau &= \frac{\mu_s}{nk_BT}\frac{1}{1+\frac{2}{5}nV_0\chi},\\
\mathrm{Pr} &= \frac{5k_B}{2m}\frac{1+\frac{3}{5}nV_0\chi}{1+\frac{2}{5}nV_0\chi}\frac{\mu_s}{\kappa}.
\end{aligned} \tag{2.20}$$

Consequently, τ and Pr depend on the appropriate determination of the shear viscosity μ_s and thermal conductivity κ of the fluids, which will be discussed in §§ 2.3.

It should be noted that the hydrostatic pressure p in (2.19) satisfies the van der Waals-type

EoS, where both the volume exclusion and the intermolecular attraction are considered. The specific form of the EoS depends on the choice of the radial distribution function χ. If we choose $\chi = 1/(1 - nV_0)$, the hydrostatic pressure (A 19) recovers the exact van der Waals EoS (1.1). However, the shielding effect of the gas molecules is not taken into account by this choice. Based on the revised Enskog theory (van Beijeren & Ernst 1973), the radial distribution function can be evaluated at a non-local density over the contact point of two colliding molecules considering the shielding effect (Carnahan & Starling 1969), which can be written as

$$\chi(\bar{n}) = \frac{1 - 0.5\eta}{(1-\eta)^3}, \quad \eta = 0.25\bar{n}V_0, \tag{2.21}$$

where $\bar{n} = \int w(\boldsymbol{r}')n(\boldsymbol{r} + \boldsymbol{r}')\mathrm{d}\boldsymbol{r}'$ (Tarazona 1985) is the local average density. Substituting (2.21) into (A 19), we can get the hydrostatic pressure p satisfying the following EoS

$$p = nk_B T \frac{1 + \eta + \eta^2 - \eta^3}{(1-\eta)^3} - an^2. \tag{2.22}$$

Clearly, this hydrostatic pressure (equilibrium) shows that our kinetic model (2.16) is thermodynamically consistent.

2.3. *Transport coefficients for van der Waals fluids*

The transport coefficients in (2.8) and (2.9) are obtained through the first order Chapman-Enskog expansion of the Enskog equation, which include both the kinetic and collisional contributions. For simplicity, the derivation of (2.8) and (2.9) was based on the hard-sphere molecules, i.e. all intermolecular collisions are rigid and elastic. To improve the accuracy of the predictions for real gases, the molecular dimensions are assumed to change with temperature, i.e., a higher temperature leads to a smaller molecular diameter, which has been widely adopted in MET (Hanley *et al.* 1972), kinetic reference theory (Karkheck & Stell 1981), and other models (Guo *et al.* 2005, 2006; Shan *et al.* 2020). This modification accounts for the softness of molecules during the collision, but the effect of the gas molecular attraction on transport coefficients is still not considered. In contrast to the Enskog equation, which describes dynamics of hard-sphere gases, no molecular potential model appears explicitly in our kinetic model (2.16). Instead, the intermolecular potential including molecular attraction for real gases is included in the transport coefficients.

For different molecular potential models (Chapman & Cowling 1990), the shear viscosity of real dilute gases can be written as

$$\mu_0 = \frac{\mu_0^{hs}}{\Omega^{(2,2)}}, \quad \mu_0^{hs} = \frac{5}{16\sigma^2}\sqrt{\frac{mk_BT}{\pi}}, \tag{2.23}$$

where μ_0^{hs} is the viscosity of dilute gases of hard-sphere molecules, and $\Omega^{(2,2)}$ is the transport collision integral depending on the intermolecular potential, which accounts for the effect of gas molecular attraction on viscosity and is difficult to obtain theoretically. Neufeld *et al.* (1972) proposed an empirical form of the integral that performs well (with error less than 0.1%) in the temperature range of $0.3 \leqslant \hat{T} \leqslant 100$ with $\hat{T} = k_BT/\epsilon$, which can be written as

$$\Omega^{(2,2)} = \frac{c_1}{\hat{T}^{c_2}} + c_3\exp(c_4\hat{T}) + c_5\exp(c_6\hat{T}) + c_7\hat{T}^{c_8}\sin(c_9\hat{T}^{c_{10}} + c_{11}), \tag{2.24}$$

with corresponding coefficients given in table 1.

To obtain the shear viscosity and thermal conductivity of van der Waals fluids, we use the method proposed by Chung *et al.* (1984, 1988), which is based on the kinetic theory and experimental correlation. For convenience, we convert the original expression to the

c_1	c_2	c_3	c_4	c_5	c_6
1.16145	0.14874	0.52487	-0.7732	2.16178	-2.43787
c_7	c_8	c_9	c_{10}	c_{11}	
-0.0006435	0.14874	18.0323	-0.7683	-7.27371	

Table 1: Coefficients for calculating of the transport integral in equation (2.24).

i	$a_0(i)$	$a_1(i)$
1	6.32402	50.4119
2	0.0012102	−0.0011536
3	5.28346	254.209
4	6.62263	38.0957
5	19.7454	7.63034
6	−1.89992	−12.5367
7	24.2745	3.44945
8	0.79716	1.11764
9	−0.23816	0.067695
10	0.068629	0.34793

Table 2: Coefficients for calculating the viscosity of van der Waals fluids in (2.26).

following form where the shear viscosity can be calculated as

$$\mu_s = \mu_0^{hs}\left(\frac{F_A F_B}{\Omega^{(2,2)}} + F_c\right), \tag{2.25}$$

with

$$F_A = 1 - 0.2756\omega, \tag{2.26a}$$
$$F_B = \frac{1}{G_v} + A_6\eta, \tag{2.26b}$$
$$F_C = \frac{1}{\hat{T}^{\frac{1}{2}}} A_7\eta^2 G_v \exp(A_8 + \frac{A_9}{\hat{T}} + \frac{A_{10}}{\hat{T}^2}), \tag{2.26c}$$
$$G_v = \frac{A_1/\eta[1-\exp(-A_4\eta)] + A_2\chi\exp(A_5\eta) + A_3\chi}{A_1A_4 + A_2 + A_3}, \tag{2.26d}$$

where F_A accounts for the effect of acentric of molecules with ω being the acentric factor, F_B and F_C account for the dependence of viscosity on gas density. For monatomic gases, the acentric factor is $\omega = 0$ so that $F_A = 1$. The coefficients $A_1 - A_9$ can be calculated by

$$A_i = a_0(i) + a_1(i)\omega, \tag{2.27}$$

with the corresponding constants shown in table 2.

Similarly, the thermal conductivity of dilute gases can be calculated as

$$\kappa_0 = \frac{\kappa_0^{hs}}{\Omega^{(2,2)}}, \quad \kappa_0^{hs} = \frac{75k_B}{64m\sigma^2}\sqrt{\frac{mk_BT}{\pi}}. \tag{2.28}$$

The thermal conductivity of van der Waals fluids at high densities can be calculated as

$$\kappa = \kappa_0^{hs}\left(\frac{F_P F_A F_D}{\Omega^{(2,2)}} + F_E\right), \tag{2.29}$$

Rapids articles must not exceed this page length

i	$b_0(i)$	$b_1(i)$
1	2.41657	0.74824
2	−0.50924	−1.50936
3	6.61069	5.62073
4	14.5425	−8.91387
5	0.79274	0.82019
6	−5.8634	12.8005
7	81.171	114.158

Table 3: Coefficients to calculate the thermal conductivity of van der Waals fluids in (2.30).

with

$$F_D = \tfrac{1}{G_t} + B_6\eta, \tag{2.30a}$$

$$F_E = 0.8906 B_7 \eta^2 G_t, \tag{2.30b}$$

$$G_t = \tfrac{B_1/\eta[1-\exp(-B_4\eta)]+B_2\chi\exp(B_5\eta)+B_3\chi}{B_1B_4+B_2+B_3}, \tag{2.30c}$$

where F_P accounts for the polyatomic effect on thermal conductivity, which is unity for monatomic gases, F_D and F_E account for the dependence of thermal conductivity on density, and the coefficients $B_1 - B_7$ can be calculated from

$$B_i = b_0(i) + b_1(i)\omega \tag{2.31}$$

using the constants shown in table 3.

Since the correlated density-dependent functions are introduced to extend the Enskog model (2.8) and (2.9) to real gases by taking gas molecular attraction into account, we refer to this modified Enskog model (2.25) and (2.29) as the correlated Enskog model in this study. Once the shear viscosity μ_s and thermal conductivity κ are calculated from (2.25) and (2.29) respectively, the relaxation time τ and Prandtl number Pr can be determined through equation (2.20).

One last parameter that needs to be determined is the bulk viscosity μ_B, which was derived for hard-sphere fluids as

$$\mu_B^{hs} = (nV_0)^2\chi\mu_0^{hs}. \tag{2.32}$$

This equation overestimates the bulk viscosity of dense LJ fluids according to Hoover *et al.* (1980*a*) and Borgelt *et al.* (1990). This overestimation is inherent in the calculation of the shear viscosity and thermal conductivity of the Enskog predictions given by (2.8) and (2.9), as these two transport coefficients are a combination of kinetic and collisional contributions. Taking the shear viscosity (2.8) as an example, equation (2.8) can be rewritten as

$$\mu^{hs} = \underbrace{\frac{\mu_0^{hs}}{\chi}\left(1+\frac{2}{5}nV_0\chi\right)}_{\mu_k} + \underbrace{\frac{\mu_0^{hs}}{\chi}\left(1+\frac{2}{5}nV_0\chi\right)\frac{2}{5}nV_0\chi + \frac{3}{5}\mu_B^{hs}}_{\mu_c}, \tag{2.33}$$

where μ_k and μ_c are the kinetic and collisional contributions to the shear viscosity, respectively. An overestimation of the bulk viscosity in the μ_c will naturally lead to an overestimation of the shear viscosity, especially at high densities where μ_c dominates. This explains the poor performance of the Enskog prediction of the transport coefficients at high densities.

Gray & Rice (1964) proposed an explicit formula for the bulk viscosity, suggesting that the bulk viscosity consists of three parts: the hard-core collision part μ_B^{hs}, the long-range attractive part μ_B^{att}, and the cross (intermediate) part μ_B^{crs} between hard-core collision and long-range attraction, namely $\mu_B = \mu_B^{hs} + \mu_B^{att} + \mu_B^{crs}$. There are conflicting explanations for this formula. Madigosky (1967) stated that the cross part μ_B^{crs} is negligible when $\hat{T} > 1$ and the long-rang attractive part $\mu_B^{att} \propto \rho^2$, which is always positive. On the contrary, Collings & Hain (1976) found that the cross part μ_B^{crs} cannot be neglected and the long-range-attractive part can be negative at high densities, which is consistent with the fact that the Enskog prediction of the transport coefficients is much larger than the experimental values at high densities, where the contribution of the long-range molecular attraction to the bulk viscosity is ignored.

A two-parametric function has recently been proposed by Chatwell & Vrabec (2020) to calculate the bulk viscosity, which is in good agreement with the experimental data and the MD simulation results at ultra-low temperature and ultra-high density conditions. However, it may become problematic when the density reduces or temperature increases, as nonphysical bulk viscosity would appear. Overall, the bulk viscosity for dense monatomic gases needs further investigation. Here, we adopt an empirical approach (Hoover *et al.* 1980*b*) to the calculation of the bulk viscosity, which considers the effect of attraction between gas molecules as

$$\mu_B = nV_0 y \left(\frac{\epsilon}{k_B T}\right)^{\frac{1}{12}} \mu_0^{hs}, \tag{2.34}$$

with

$$y = 2.722x + 3.791x^2 + 2.495x^3 - 1.131x^5, \tag{2.35a}$$

$$x = 0.477465 nV_0 \left(\frac{\epsilon}{k_B T}\right)^{\frac{1}{4}}. \tag{2.35b}$$

To be consistent with the shear viscosity and thermal conductivity, we refer to this equation (2.34) as the correlated Enskog model since the effect of gas molecular attraction is included.

3. Numerical results and discussion

Here, we examine whether our kinetic model (2.16) can capture the non-equilibrium and dense gas effects of surface-confined flows of van der Waals fluids. The kinetic model is solved by the discrete velocity method together with the diffuse boundary condition, which is set at the position a half-molecule size away from the physical boundary as the molecule dimension is considered (see figure 1). The steady-state solutions are obtained using a semi-implicit iteration scheme (Su *et al.* 2020), with the flow field initialised at the equilibrium state.

MD simulations are conducted to validate the current kinetic model. In the MD simulations, fluid molecules interact with each other through the LJ potential (1.2). For initialisation, molecular velocities are generated with a Gaussian distribution to produce the required temperature, followed by a run of 5×10^4 steps in the NVT system to ensure that the initial states (mass, momentum, and energy) are the same for the MD and the kinetic simulations. Afterwards, the NVE system is employed to run all the cases with sufficient time steps and obtain the flowfield data. The energy and size (molecule diameter) parameters are obtained through the critical temperature and volume of the fluids (Chung *et al.* 1988), respectively, as

$$\epsilon = \frac{k_B T_c}{1.2593}, \tag{3.1a}$$

$$\sigma = \left(\frac{M V_c}{N_A \pi}\right)^{\frac{1}{3}}, \tag{3.1b}$$

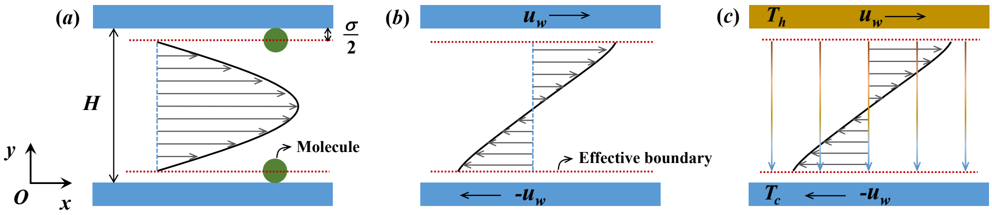

Figure 1: Schematic of (*a*) Poiseuille, (*b*) Couette, and (*c*) Couette-Fourier flows.

where T_c is the critical temperature (K), σ is the molecular diameter (m), $V_c = 1/\rho_c$ is the critical volume (m^3/kg), M is the molar mass (kg/mol), and N_A is the Avogadro constant. For argon, the critical temperature $T_c = 150.69$ K and the critical density $\rho_c = 535.60$ kg/m^3 are chosen in this study.

We consider the van der Waals fluids confined between two parallel plates located at $y = 0$ and $y = H$ respectively, as shown in figure 1. In Poiseuille flow, the plates are kept stationary and all the fluid molecules are subjected to an external force $\boldsymbol{F}_{ext}$ in the x direction. In Couette and Couette-Fourier flows, the top and bottom plates move with velocity u_w and $-u_w$ in the opposite directions, which drive fluid molecules to move. In Poiseuille and Couette flows, the temperatures of the top and bottom plates are identical, while the temperature of the top plate temperature T_h is higher than the bottom plate T_c in Couette-Fourier flow.

3.1. *Model analysis and comparison*

The radial distribution function plays an essential role in the MET. A key requirement for determining the radial distribution function is that $\chi \to 1$ as $n \to 0$, so that the Enskog equation for dense gases reduces to the Boltzmann equation in the dilute limit. However, the MET does not satisfy this requirement when the van der Waals pressure is chosen, as shown by equation (1.4), which makes the MET inaccurate in capturing the effect of the long-range molecular attraction. A temperature-dependent diameter (Hanley *et al.* 1972) can be employed to correct this problem, which relates the covolume V_0 with the second virial coefficient B through $V_0 = B + T\mathrm{d}B/\mathrm{d}T$, and leads directly to the following EoS for real gases

$$p = Znk_BT, \quad Z = 1 + n\chi(B + T\frac{\mathrm{d}B}{\mathrm{d}T}), \tag{3.2}$$

where Z is the compressibility factor. Clearly, the real gas EoS recovers the ideal gas EoS as the compressibility factor $Z \to 1$ when $n \to 0$. However, the compressibility factor Z may be less than unity near the critical temperature, which means that the radial distribution function χ may be negative in (3.2) as both $n > 0$ and $V_0 = B + T\mathrm{d}B/\mathrm{d}T > 0$, thus leading to negative shear viscosity and thermal conductivity, as can be seen from (2.8) and (2.9), which is physically inappropriate. Therefore, the MET is not suitable for modelling gas dynamics of van der Waals fluids.

As shown in figure 2, the Enskog prediction overestimates the shear viscosity and thermal conductivity at high densities. The assumption of a state-dependent diameter (2.7) attenuates this overestimation at low temperatures, see figure 2(*a*), but leads to an overestimation of the shear viscosity at low densities, see figure 2(*b*). Overall, the correlated Enskog model agrees well with the experimental data for a wide range of temperatures and densities, particularly for shear viscosity and thermal conductivity, which indicates the accuracy of taking the molecular attraction into account to calculate the transport coefficients.

Similar to the shear viscosity and thermal conductivity, it improves the prediction accuracy by taking the molecular attraction into account to calculate the bulk viscosity. However, the

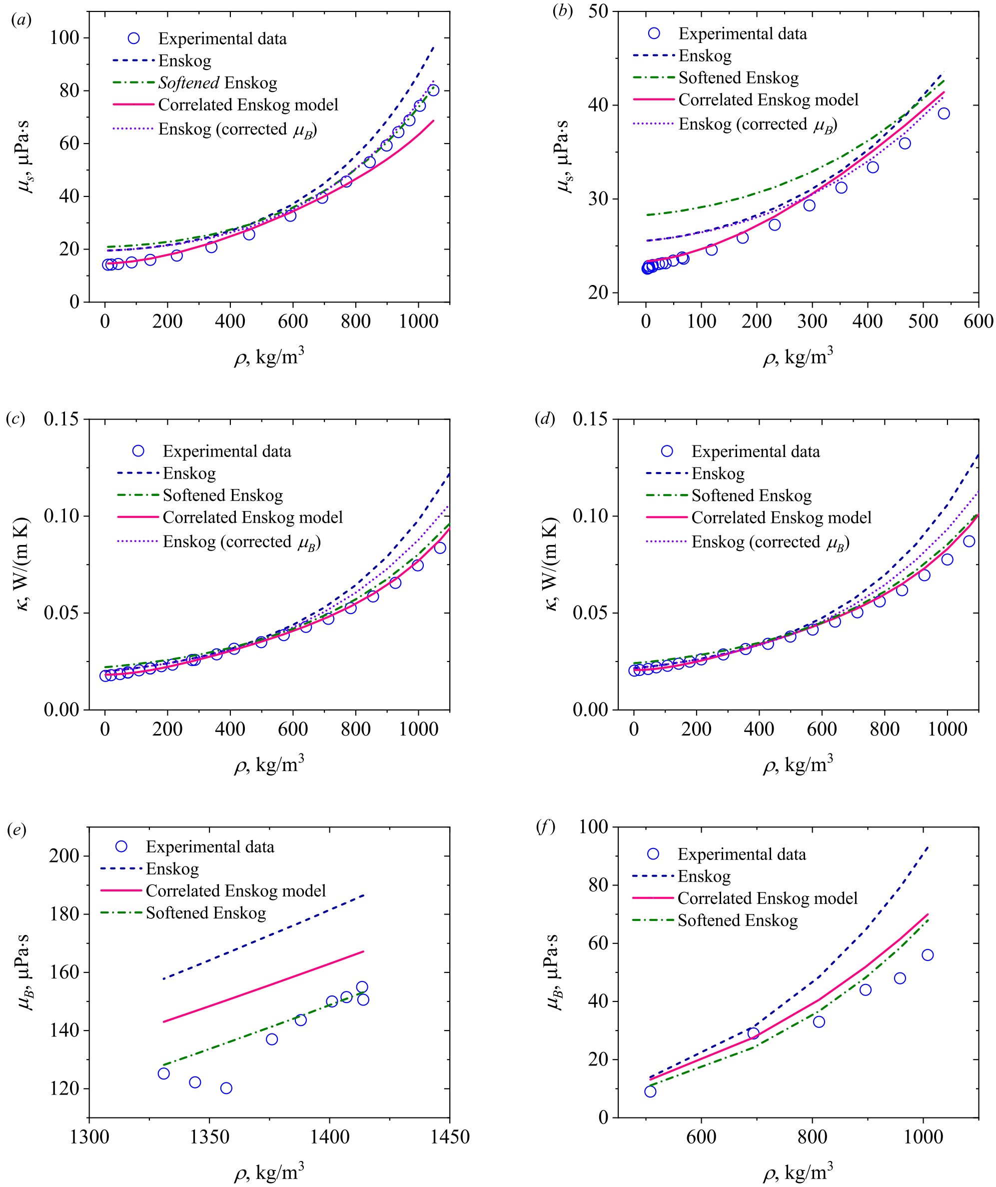

Figure 2: Comparison of transport coefficients: (*a*) and (*b*) for the shear viscosity at T = 173.0 K and 298.0 K, respectively, with the experimental data from Haynes (1973); (*c*) and (*d*) for the thermal conductivity at T = 298.15 K and 348.15 K, respectively, with the experimental data from Michels *et al.* (1963); and (*e*) and (*f*) for the bulk viscosity with the experimental data from Malbrunot *et al.* (1983) and Madigosky (1967), respectively. The correlated Enskog model considers the effect of gas attraction on shear viscosity and thermal conductivity using the approach of Chung *et al.* (1988), and on bulk viscosity using the approach of Hoover *et al.* (1980*b*). The *softened* Enskog uses a state-dependent molecule diameter (2.7) in the Enskog prediction of transport coefficients (2.32). The Enskog (corrected μ_B) uses the corrected bulk viscosity in the Enskog prediction of shear viscosity (2.33).

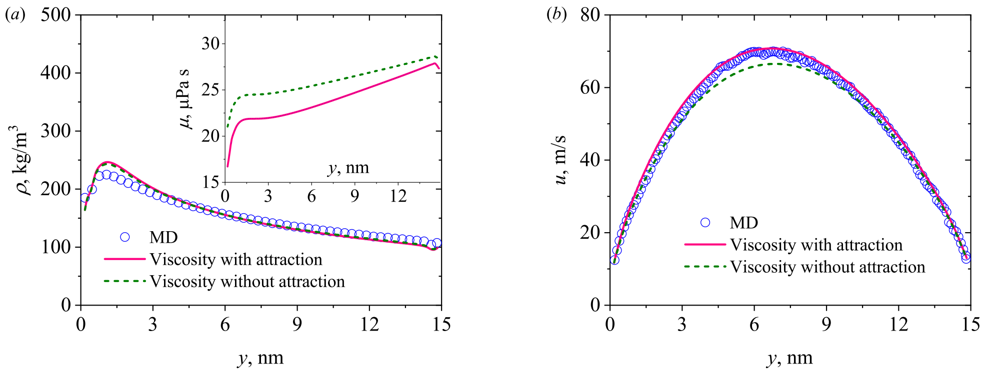

Figure 3: The effect of viscosity models on (a) density and viscosity and (b) velocity profiles, where the viscosity without attraction refers to the hard-sphere model (2.8) and viscosity with attraction refers to the Chung model (2.25).

bulk viscosity is more accurately predicted using the Enskog prediction formula (2.32) with a state-dependent diameter (2.7), i.e. the *softened* Enskog prediction, as shown in figure 2(*e*) and (*f*). Consequently, the Enskog prediction of shear viscosity and thermal conductivity is in better agreement with the experimental data at high densities if we take this corrected bulk viscosity into (2.33) to replace the original hard-sphere bulk viscosity μ_B^{hs}, see figure2(*a*), (*b*), (*c*) and (*d*), which proves that the overestimation of bulk viscosity from the Enskog theory leads to the overestimation of the shear viscosity and thermal conductivity, see figure2(*a*), (*b*), (*c*) and (*d*), at high densities.

The effect of viscosity models on gas density, viscosity and velocity distributions is shown in figure 3, where a Poiseuille-type flow is investigated with the bottom and top wall temperatures T_c = 173 K and T_h = 373 K, respectively, the averaged density ρ_{avg} = 150 kg/m^3, the channel width H = 15 nm, and the external force F_{ext} = 0.0003 kcal/(mol Å). Although the viscosity model barely affects the density distribution, it is more accurate to predict the flow velocity profile when the molecular attraction is taken into account. The tendency of viscosity and density across the channel is opposite since the viscosity is dominated by temperature at a relatively low density.

The present kinetic model (2.16) will then be evaluated by comparison with the simulation results of MD, the Shakhov-Enskog model (Wang *et al.* 2020), and the NS equations. For incompressible, steady state and laminar flows, the NS equations reduces to

$$\mu \frac{\partial^2 u}{\partial y^2} + F_{ext} n = 0, \tag{3.3a}$$

$$\kappa \frac{\partial^2 T}{\partial y^2} + \mu \left(\frac{\partial u}{\partial y} \right)^2 = 0, \tag{3.3b}$$

with the second-order boundary condition for velocity slip and the first-order boundary condition for temperature jump, namely

$$u_s = \pm A_1 \lambda \frac{\partial u}{\partial y}|_{y=0} - A_2 \lambda^2 \frac{\partial^2 u}{\partial y^2}|_{y=0}, \tag{3.4a}$$

$$T_j = \beta \frac{2\gamma}{\gamma+1} \frac{\lambda}{\mathrm{Pr}} \frac{\partial T}{\partial y}|_{y=0}, \tag{3.4b}$$

where the slip coefficients A_1 = 1.0 and A_2 = 0.5 are chosen (Chapman & Cowling 1990), and $\beta = (2 - \sigma_T)/\sigma_T$ with the chosen thermal accommodation coefficient σ_T = 1.0.

3.2. *Poiseuille flows*

In Poiseuille flows, an external body force is acted on all the fluid molecules in the x direction with the wall temperature $T_w = 273K$. By solving (3.3) and (3.4), the velocity and temperature distribution across the channel can be obtained as

$$u(y) = -\tfrac{F_{ext}n}{2\mu}[y^2 - yH - H^2(A_1\mathrm{Kn} + 2A_2\mathrm{Kn}^2)], \tag{3.5a}$$

$$T(y) = -\tfrac{(F_{ext}n)^2}{24\mu\kappa}(2y^4 - 4Hy^3 + 3H^2y^2 - H^3y - L_TH^4) + T_w, \tag{3.5b}$$

where Kn is the Knudsen number defined as

$$\mathrm{Kn} = \frac{1}{\sqrt{2}n\pi\sigma^2\chi H}. \tag{3.6}$$

Figure 4 shows the density and velocity profiles of the Poiseuille flows under a small external body force at different densities, i.e. different degrees of non-equilibrium (rarefaction) effect. As shown, the results of our kinetic model are in good agreement with the MD data for a broad range of densities (the reduced number density η ranges from 0.00031 to 0.14). In contrast, the Shakhov-Enskog model (Wang *et al.* 2020), which neglects the gas molecular attraction, overestimates the density near the wall and underestimates the overall velocity profiles, particularly at high densities. The NS prediction, on the other hand, is better at high densities where the non-equilibrium effect is not significant.

For high-speed flows, the viscous dissipation plays an important role, which is investigated in figure 5 with the average density $\rho_{avg} = 350$ kg/m^3, channel width $H = 5$ nm, and wall temperature $T_w = 273$ K. Two large external forces are considered, namely $F_{ext} =$ 0.01 and 0.02 kcal/(mol Å), respectively. Again, the density oscillation, parabolic velocity, and quartic temperature profiles are well captured by the current kinetic model, while the Shakhov-Enskog model and the NS equation show large errors. The discrepancy in the results between the current kinetic model and the Shakhov-Enskog model suggests the important role of the long-range molecular attraction in gas dynamics, leading to reduced density near the wall, and enhanced velocity slip and temperature jump.

The effect of temperature on density and velocity profiles is shown in figure 6, with the average density $\rho_{avg} = 350$ kg/m^3, channel width $H = 5$ nm, and external force $F_{ext} =$ 0.001 Kcal/(mol Å). It is very clear that the density and velocity profiles predicted by our kinetic model agree with the MD data, while the NS equation fails to predict density variation and the Shakhov-Enskog model overpredicts the density near the wall. The main difference between our model and the Shakhov-Enskog model is that we include the gas molecular attraction, which can hold the gas molecules to the bulk. As a result, our prediction of the density at the wall is significantly smaller than the Shakhov-Enskog model for hard-sphere molecules which ignores the molecular attraction. As shown by figure 6(*e*), even at high temperatures, the gas density of van der Waals fluids is still significantly affected by the long-range molecular attraction, i.e. the gas molecular attraction is not negligible even at high temperatures, which has rarely been reported in previous studies.

The velocity decreases with the temperature, as shown by figure 6(*b*), (*d*) and (*f*), which is caused by the higher near-wall density and lager viscosity at high temperatures. The higher near-wall density means more efficient momentum transfer between the fluid and the wall, leading to less velocity slip at the boundary, while a higher viscosity means more flow resistance for bulk gas flows in the channel. This can be more clearly seen by normalising the slip velocity u_s by $F_{ext}H/(mu_m)$, namely

$$\hat{u}_s = \frac{u_s m u_m}{F_{ext}H}, \quad u_m = \sqrt{\frac{2k_BT}{m}}, \tag{3.7}$$

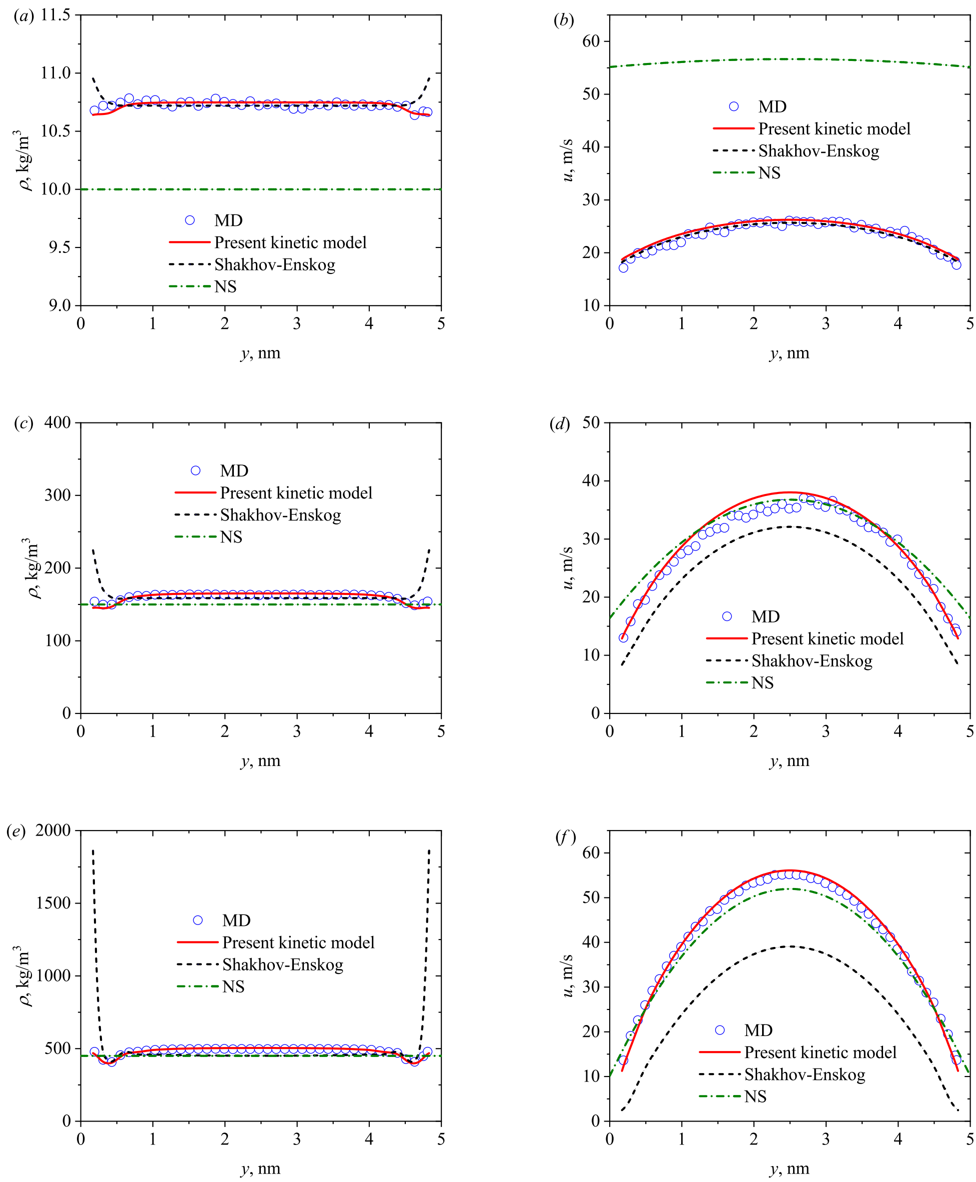

Figure 4: Density and velocity profiles at: (*a*) and (*b*) for ρ_{avg} = 10 kg/m^3 (η = 0.00031, Kn = 2.56); (*c*) and (*d*) for ρ_{avg} = 150 kg/m^3 (η = 0.047, Kn = 0.15); and (*e*) and (*f*) for ρ_{avg} = 450 kg/m^3 (η = 0.14, Kn= 0.039). The external force F_{ext} = 0.001 kcal/(mol Å) is small so that the viscous dissipation is negligible, the channel width is H =5 nm, and the wall temperature is 273 K.

where u_m is the most probable velocity. The variation of the normalised slip velocity with temperature is shown in figure 7. The normalised slip velocity of hard-sphere gases predicted by the Shakhov-Enskog model is nearly constant as the temperature changes, while the present kinetic model and MD simulation predict a decreasing slip velocity with temperature. For hard-sphere gases, the density distribution is not affected by the temperature, and the

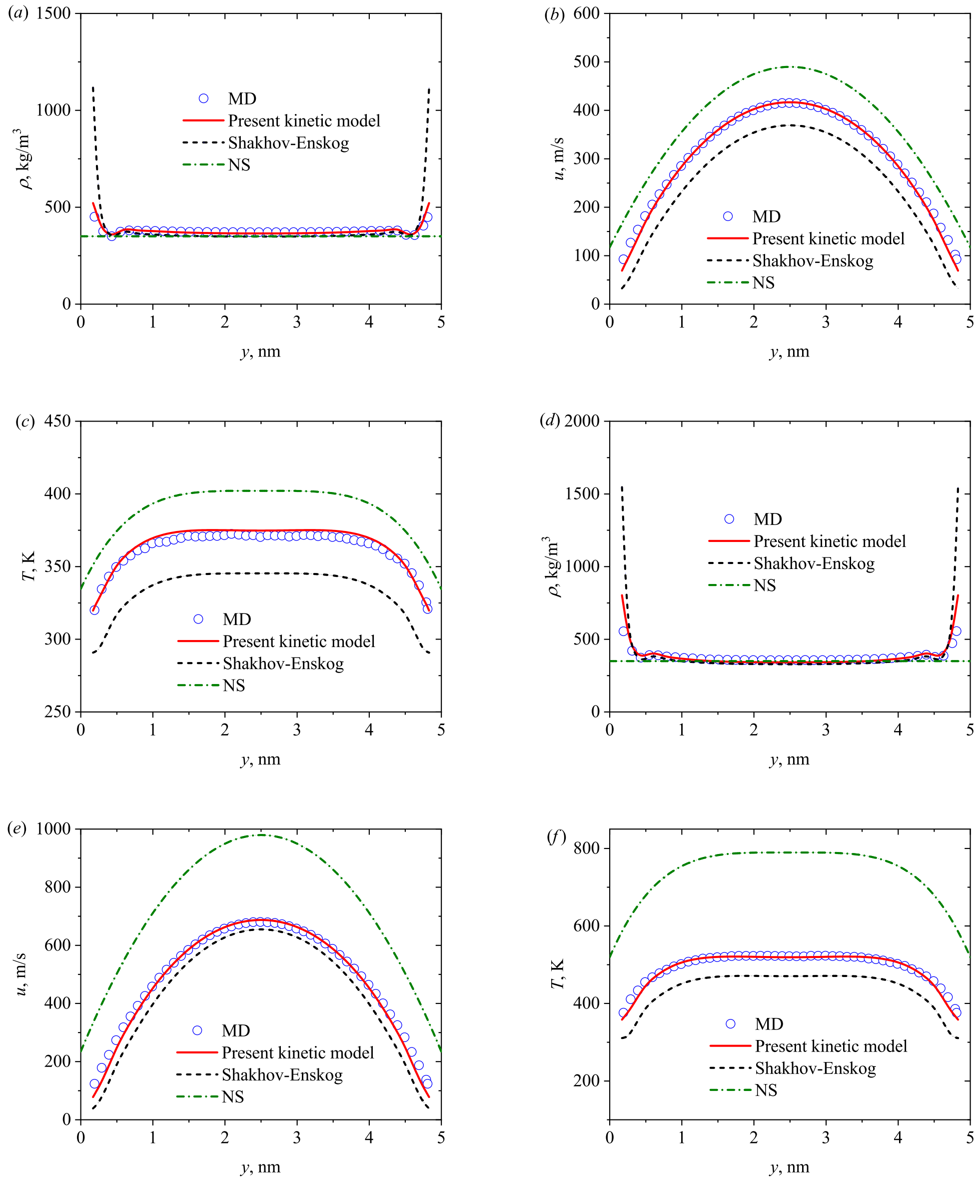

Figure 5: Density, velocity and temperature profiles at different external forces: (a), (b) and (c) for F_{ext} = 0.01 kcal/(mol Å); and (d), (e) and (f) for F_{ext} = 0.02 kcal/(mol Å). The average density is ρ_{avg} = 350 kg/m^3 (η =0.11), the channel width is H =5 nm, and the wall temperature is T_w = 273 K. The resulting Knudsen number is Kn=0.055.

velocity distribution $u(y) \propto 1/\mu_s^{hs}$. As shown by (2.8), the viscosity $\mu_s^{hs} \propto \sqrt{T}$, so the normalised velocity is temperature independent as $u_m \propto \sqrt{T}$. However, the relationship between viscosity and temperature $\mu_s \propto \sqrt{T}$ no longer holds for van der Waals fluids as the transport collision integral $\Omega^{(2,2)}$, which is temperature dependent, comes into play. Furthermore, a new dimensionless number, namely the reduced temperature $\hat{T} = k_B T/\epsilon$ is introduced to signify the competition between gas molecular attraction and kinetic energy for van der Waals

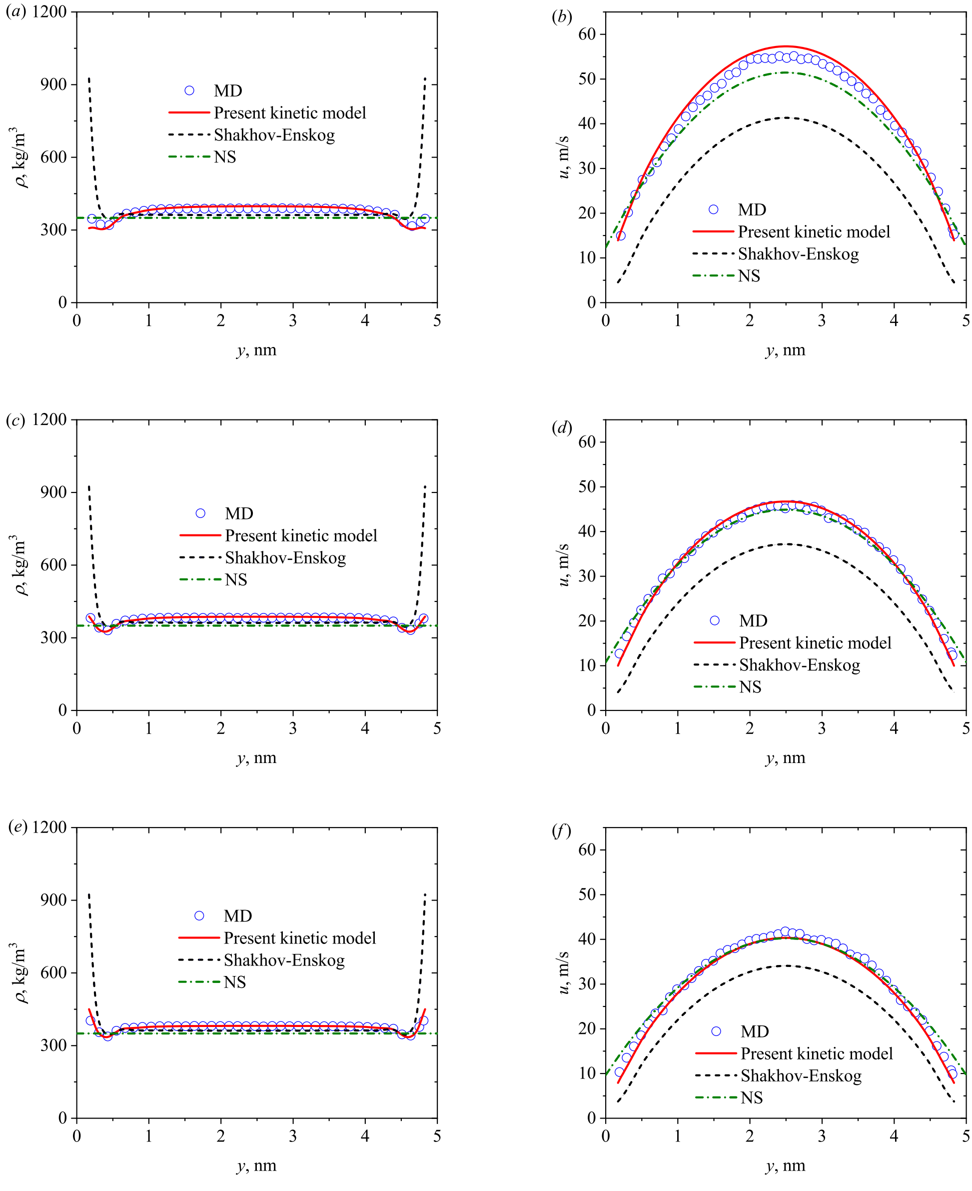

Figure 6: Density and velocity profiles at different temperatures: (*a*) and (*b*) for T = 253 K; (*c*) and (*d*) for T = 313 K; and (*e*) and (*f*) for T = 373 K. The average density is ρ_{avg} = 350 kg/m^3, the channel width is H =5 nm, and the external force F_{ext} = 0.001 kcal/(mol Å).

fluids. As the temperature increases, the gas molecules gain more kinetic energy to overcome the attraction holding them in the bulk. This results in greater accumulation near the walls, leading to increased momentum transfer between the solid and the gas, thus reducing the slip velocity.

As the viscous dissipation is non-negligible for fluids under high shear rates, we investigate

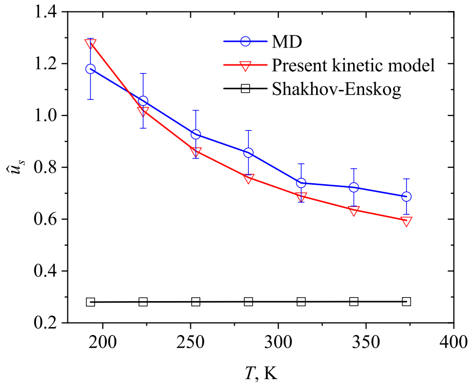

Figure 7: The variation of the normalised slip velocity with temperature.

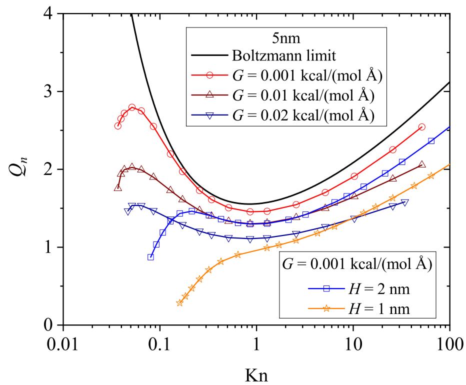

Figure 8: The variation of normalised mass flow rate with the Knudsen number at different external forces and confinements.

its effect on the normalised mass flow rate Q_n, which is defined as

$$Q_n = \frac{\int_0^H n(y)y(y)\mathrm{d}y}{n_{avg}F_{ext}H^2/(mu_m)}. \tag{3.8}$$

As shown in figure 8, increased viscous dissipation reduces the mass flow rate in all the flow regimes. This is because the viscous dissipation leads to a smaller slip velocity and larger flow resistance, as shown by the results in figure 5. The effect of viscous dissipation on mass flow rate is similar to that of confinement, which is also included in figure 8 for comparison. However, the confinement reduces the mass flow rate more significantly for small-Kn flows, resulting in the disappearance of the Knudsen minimum. On the contrary, the viscous dissipation flattens the variation curve ($Q_n \sim$ Kn), but no Knudsen minimum disappearance is observed.

3.3. *Couette flows*

In Couette flows, the top and bottom walls move in opposite directions at the speed of u_w in the opposite directions, as shown in figure 1(b). No external force is exerted on fluid molecules, so $F_{ext} = 0$ and the wall temperature is set to be $T_w = 273$ K. The velocity and temperature profiles can also be obtained by solving (3.3) and (3.4), which are written as

$$u(y) = \tfrac{2u_w}{H} y - u_w, \tag{3.9a}$$

$$T(y) = -\tfrac{2\mu u_w^2}{\kappa H^2}\left(y^2 - Hy - H^2\beta\tfrac{2\gamma}{\gamma+1}\tfrac{\mathrm{Kn}}{\mathrm{Pr}}\right) + T_w. \tag{3.9b}$$

Figure 9 shows the density, velocity, and temperature profiles of the Couette flows at different shear rates, with the average density $\rho_{avg} = 350$ kg/m^3, and channel width $H = 5$ nm. The present kinetic model captures the density oscillation, linear velocity distribution, and parabolic temperature distribution, which are in good agreement with the MD data. Similar to the Poiseuille flows, the Shakhov-Enskog model, which neglects the long-range attraction between gas molecules, overestimates the density near the wall and underestimates both the velocity slip and the temperature jump. As the shear rate increases, gas molecules are more likely to accumulate near the wall, as the long-range molecular attraction may not be sufficient to hold the gas molecules to the bulk, also shown in figure 10. In contrast to the density peak near the wall, the viscosity is lowest in this region, see figure 10(*d*). This is because the bulk gas has higher temperatures due to the viscous heating. Figure 10(*b*) shows that stronger viscous dissipation causes a reduction in velocity slip as a combined consequence of a higher density peak and a greater viscosity near the wall.

The viscous dissipation effect on Couette flows under tighter confinement is also investigated, where the channel width shrinks from 5 nm to 2 nm, as shown in figure 11. For such a case, both the non-equilibrium and confinement effects become stronger. The results from the Shakhov-Enskog model and the NS equations exhibit larger discrepancies compared to the MD simulation results, while our kinetic model can still accurately capture the density, velocity, and temperature profiles.

3.4. *Couette-Fourier flows*

The Couette-Fourier flow differs from the Couette flow only in the different wall temperatures, with the top wall temperature at $T_h = 373$ K and the bottom wall temperature at $T_c = 273$ K. By solving (3.3) and (3.4), the velocity and temperature can be obtained as

$$u(y) = \tfrac{2u_w}{H} y - u_w, \tag{3.10a}$$

$$\tfrac{T(y)-T_c}{T_h-T_c} = -2\mathrm{Br}\left[\left(\tfrac{y}{H}\right)^2 - (1-2L_T)\tfrac{y}{H} - L_T(1-2L_T)\right] + \tfrac{y}{H} + L_T, \tag{3.10b}$$

where $\mathrm{Br} = \mu u_w^2/[\kappa(T_h - T_c)]$ is the Brinkman number measuring the competition between viscous heating and thermal conduction, and L_T is the thermal jump length, which can be obtained from the temperature jump condition as

$$L_T = \beta\frac{2\gamma}{\gamma+1}\frac{\mathrm{Kn}}{\mathrm{Pr}}. \tag{3.11}$$

The density, velocity, and temperature profiles of the Couette-Fourier flows at two different wall velocities are shown in figure 12, with the channel width $H = 5$ nm. At a small wall moving velocity (u_w =50 m/s), the viscous dissipation is negligible, so the density and temperature distributions recover that of Fourier flows, while the velocity distribution is similar to the Couette flows. When the wall velocity increases to $u_w = 300$ m/s, the temperature profile becomes a combination of the linear and parabola distributions resulting from the Fourier and Couette flows, respectively. Again, the present kinetic model accurately predicts these profiles, while the results of the Shakhov-Enskog model significantly deviate from the MD data , particularly for the density and temperature profiles.

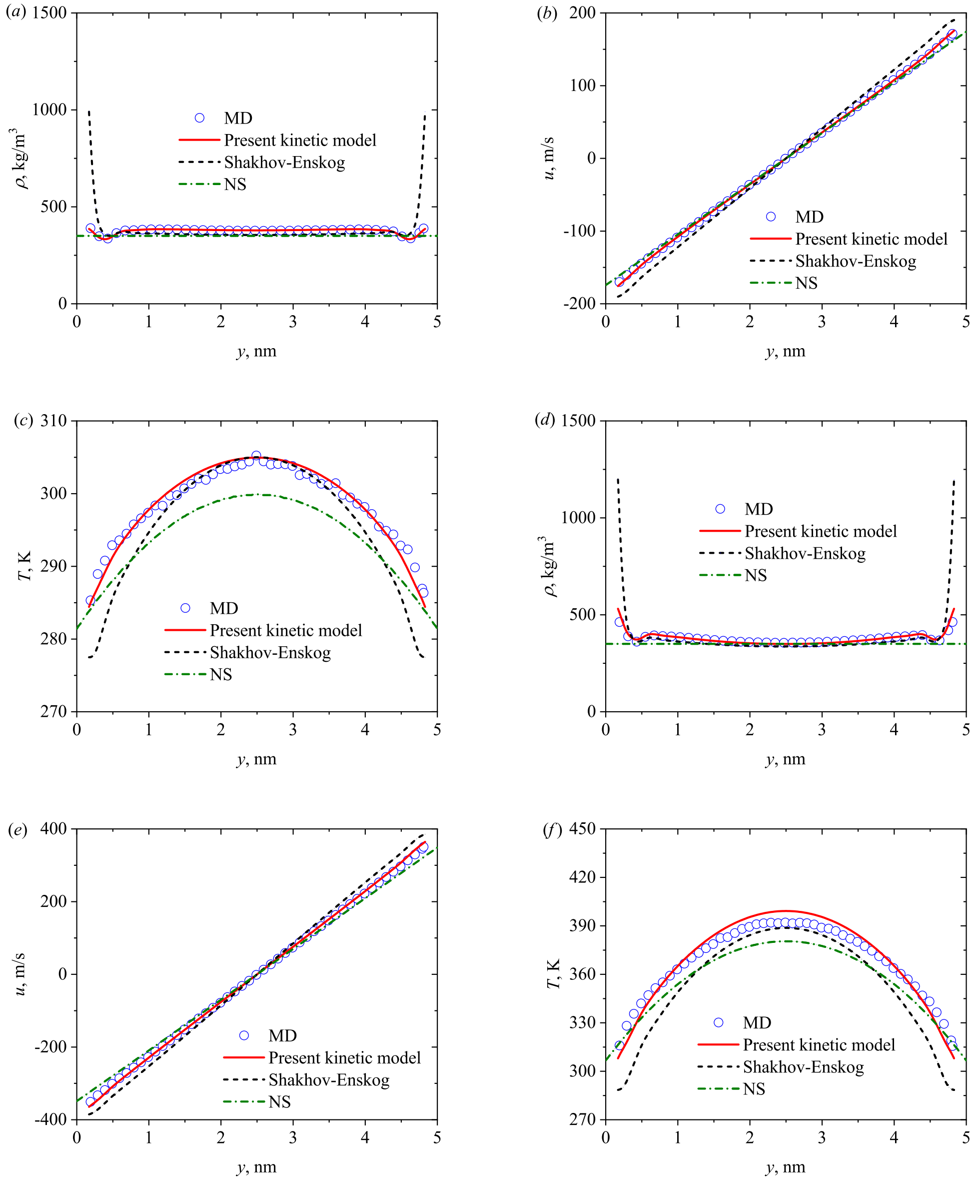

Figure 9: Density, velocity and temperature profiles: $(a-c)$ u_w = 200 m/s; and $(d-f)$ u_w = 400 m/s. The average density is ρ_{avg} = 350 kg/m^3, the channel width is H =5 nm, and the wall temperature is T_w = 273 K.

With increased viscous dissipation at high wall velocities, the heat generated in the gases leads to higher gas temperatures, as shown in figure 13(a). The viscous dissipation increases the heat transfer rate between the gas and the cold (bottom) wall, while it limits the heat transfer rate between the gas and the hot (top) wall, which can be clearly seen from the heat flux variation in figure 13(b). When the wall velocity is sufficiently large, the hot wall can also be heated by the gases due to the large amount of heat generated by viscous heating.

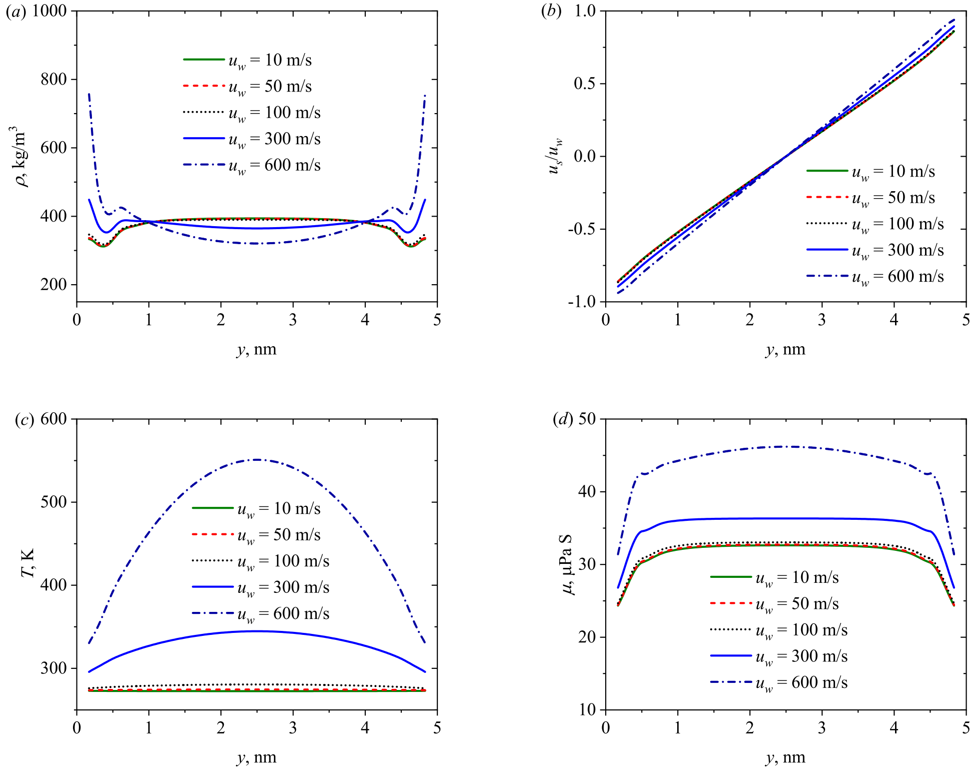

Figure 10: Distribution of density (a), velocity (b), temperature (c), and viscosity (d) across the channel at different wall velocities. The average density is ρ_{avg} = 350 kg/m^3, the channel width is H =5 nm, and the wall temperature is T_w = 273 K.

Thus, our kinetic model may provide a design simulation tool to develop next-generation technologies such as nanoscale evaporative cooling.

3.5. *Model solution in the dilute and continuum limits*

As shown in figure 14(a) and (b), the results of the present kinetic model for van der Waals fluids are in good agreement with the Shakov-Boltzmann model for dilute gases and the MD simulation when the real gas effects (namely the volume exclusion and the long-range molecular attraction) and the confinement are negligible. This is because the density terms $\mathcal{I}^{(1)}$ (2.14) and $\mathcal{I}^{(2)}$ (2.15) and the mean-field force (2.6) become negligible, and the kinetic model (2.16) reduces to the Shakhov model for hard-sphere molecules in the dilute limit. Meanwhile, the results of our kinetic model, NS equations, and MD simulations are very close in the continuum limit where the non-equilibrium and confinement effects are sufficiently small, as shown in figure 14(c) and (d). This is also expected because the NS equations are recovered from the kinetic model (2.16) in the small-Kn limit, as shown in appendix A. Therefore, the present kinetic model, which is an extension from the Enskog-Vlasov model for hard-sphere molecules to include real gas effects, is capable of simulating non-equilibrium flows of surface-confined van der Waals fluids.

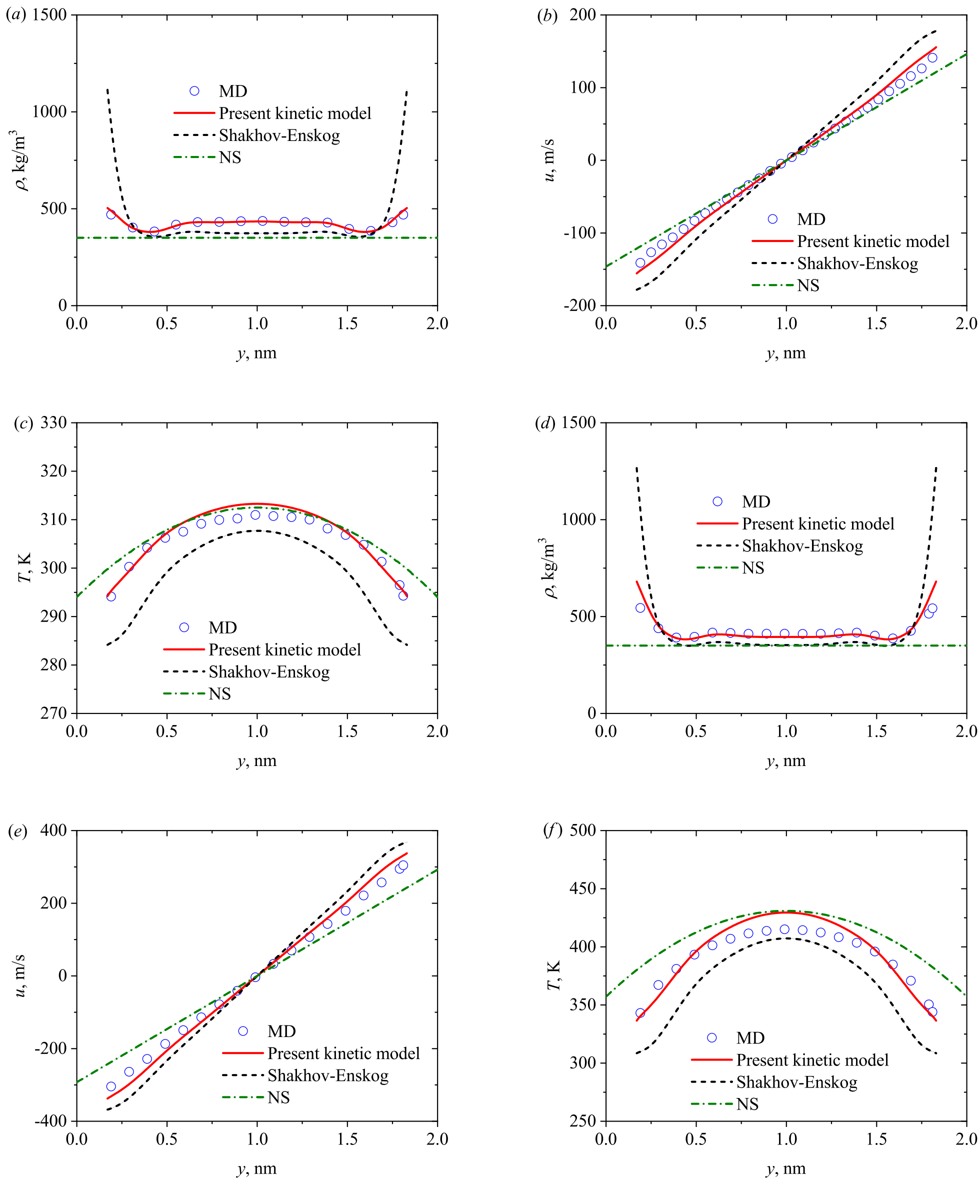

Figure 11: Density and velocity profiles at: $(a-c)$ u_w = 200 m/s; and $(d-f)$ u_w = 400 m/s. The average density is ρ_{avg} = 350kg/m^3, the channel width is H =2 nm, and the wall temperature is T_w = 273 K. The resulting Knudsen number is Kn = 0.14.

4. Conclusions

We have proposed a simplified kinetic model for surface-confined flows of van der Waals fluids, which is consistent with the Boltzmann model in the dilute limit and with the NS equations in the continuum limit. The long-range molecular attraction is taken into account both in the kinetic equation and in the transport coefficients (shear viscosity and thermal conductivity). Through the Chapman-Enskog expansion, macroscopic equations can be ob-

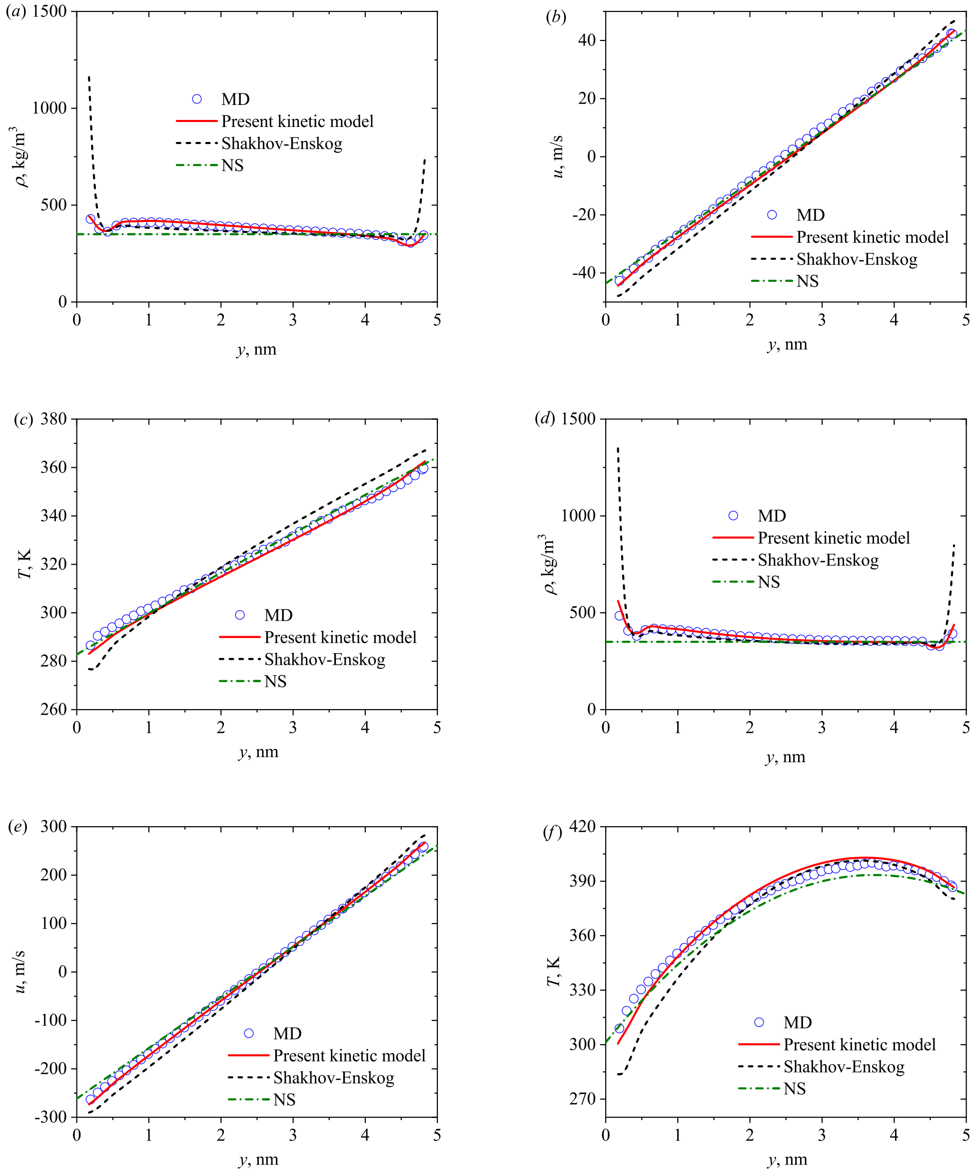

Figure 12: Density, velocity and temperature profiles of the Couette-Fourier flows at different wall velocities: $(a-c)$ $u_w = 50$ m/s; and $(d-f)$ $u_w = 300$ m/s. The average density is $\rho_{avg} = 350$ kg/m^3, the channel width is H =5 nm, and the top and bottom wall temperatures are $T_h = 373$ K and T_c=273 K, respectively.

tained with a correct form of EoS if the radial distribution function is chosen appropriately, demonstrating the thermodynamic consistency of our kinetic model.

Further analysis shows that the shear viscosity and thermal conductivity are in better agreement with the experimental data when the gas attraction is taken into account, while the bulk viscosity is more accurately predicted by the Enskog formula for hard-sphere molecules with a state-dependent diameter. The Enskog theory greatly overestimates the bulk viscosity

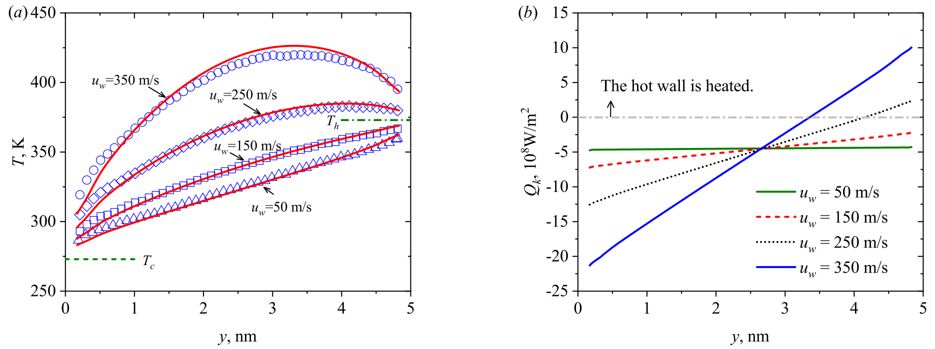

Figure 13: Temperature (a) and heat flux (b) distributions of Couette-Fourier flows at different wall velocities, where the symbols denote the MD data. The averaged density is ρ_{avg} = 350 kg/m^3, the channel width is H =5 nm, and the top and bottom wall temperatures are T_h = 373 K and T_c=273 K, respectively.

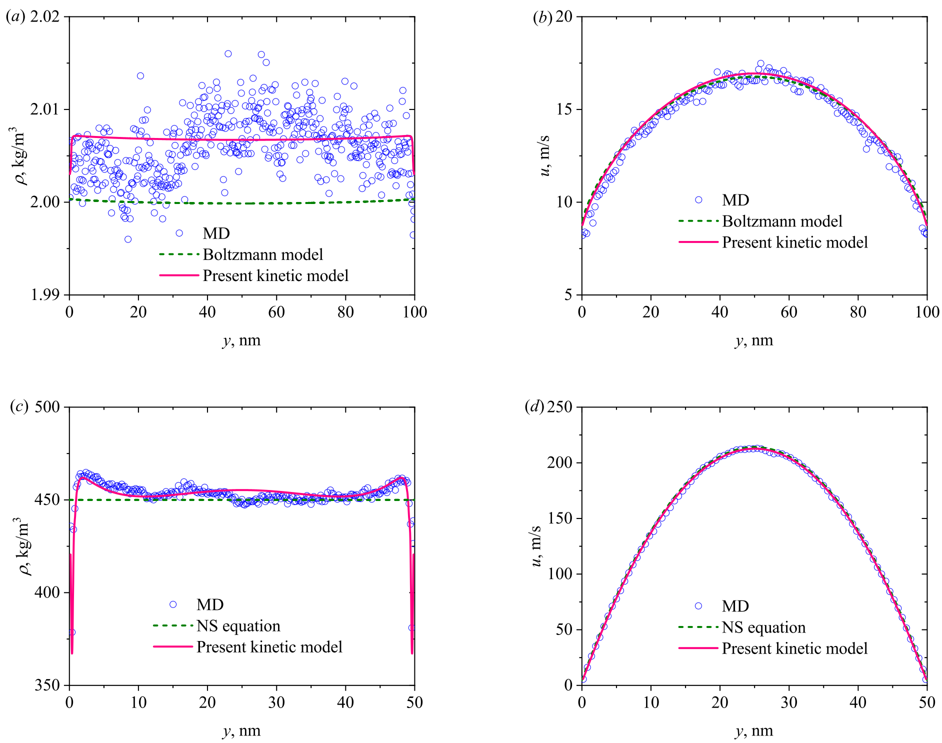

Figure 14: The present kinetic model agrees with the Boltzmann model in the dilute limit (a) and (b), and with the NS equations in the continuum limit (c) and (d). The average density ρ_{avg} = 2 kg/m^3, the channel width H =100 nm, and the external force F_{ext} = 0.00003 kcal/(mol Å) in (a) and (b), correspond to η = 0.00062 and Kn = 0.64; the average density ρ_{avg} = 450 kg/m^3, the channel width H =50 nm, and the external force F_{ext} = 0.00005 kcal/(mol Å) in (c) and (d), correspond to η = 0.14 and Kn = 0.0039.

of dense gases, which explains the overestimation of shear viscosity and thermal conductivity at high densities. The empirical MET which incorporates the gas attraction into the radial distribution function either fails to recover the Boltzmann equation in the dilute limit or produces non-physical properties, e.g. negative transport coefficients near critical temperatures. Momentum and energy transfer become temperature dependent for van der Waals fluids due to gas molecular attraction, which is not the case for hard-sphere molecules. The extensive numerical tests suggest that the present model can capture the non-equilibrium, confinement, real gas, and thermal effects simultaneously.

Acknowledgement

Supercomputing time on ARCHER is provided by the "UK Consortium on Mesoscale Engineering Sciences (UKCOMES)" under the UK Engineering and Physical Sciences Research Council Grant No. EP/R029598/1. This work made use of computational support by CoSeC, the Computational Science Centre for Research Communities, through UKCOMES.

Funding

This work is supported by the UK's Engineering and Physical Sciences Research Council (grant no. EP/R041938/1).

Declaration of interests

The authors declare no competing interests.

Appendix A. Chapman-Enskog expansion of the kinetic model

The Chapman-Enskog expansion (Chapman & Cowling 1990) is used to derive the hydrodynamic equations from the kinetic model (2.16), on the basis of which the relaxation time τ and the Prandtl number Pr can be assigned according to their relationship with the shear viscosity and thermal conductivity. First, the following expansions are introduced as

$$\begin{aligned}
\frac{\partial}{\partial t} &= \varepsilon^{(1)}\frac{\partial}{\partial t_1} + \varepsilon^{(2)}\frac{\partial}{\partial t_2},\\
\frac{\partial}{\partial \boldsymbol{r}} &= \varepsilon^{(1)}\frac{\partial}{\partial \boldsymbol{r}_1},\\
\frac{\partial}{\partial \boldsymbol{\xi}} &= \varepsilon^{(1)}\frac{\partial}{\partial \boldsymbol{\xi}_1},\\
f &= f^{(0)} + \varepsilon^{(1)} f^{(1)} + \varepsilon^{(2)} f^{(2)} + O(f^{(3)}),\\
\boldsymbol{Q}_k &= \boldsymbol{Q}_k^{(0)} + \varepsilon^{(1)}\boldsymbol{Q}_k^{(1)} + \varepsilon^{(2)}\boldsymbol{Q}_k^{(2)} + O(\boldsymbol{Q}_k^{(3)}),
\end{aligned} \tag{A 1}$$

where ε is a small parameter on the order of the Knudsen number. Following these expansions (A 1), the kinetic equation (2.16) can be transformed into a hierarchy of equations according to the order of ε, with the preceding equations given as

$$\begin{aligned}
\varepsilon^{(0)}: &\quad f^{(0)} = f^{eq}, \\
\varepsilon^{(1)}: &\quad \frac{\partial f^{(0)}}{\partial t_1} + \boldsymbol{\xi}\cdot\frac{\partial f^{(0)}}{\partial \boldsymbol{r}_1} + \frac{\boldsymbol{F}_{ext}+\boldsymbol{F}_{att}}{m}\cdot\frac{\partial f^{(0)}}{\partial \boldsymbol{\xi}_1} \\
&\qquad = -\frac{1}{\tau}\left[f^{(1)} - f^{eq}(1-\mathrm{Pr})\frac{\boldsymbol{c}\cdot\boldsymbol{Q}_k^{(1)}}{5p_0RT}\left(\frac{c^2}{RT}-5\right)\right] + \mathcal{I}^{(1)}, \\
\varepsilon^{(2)}: &\quad \frac{\partial f^{(1)}}{\partial t_1} + \frac{\partial f^{(0)}}{\partial t_2} + \boldsymbol{\xi}\cdot\frac{\partial f^{(1)}}{\partial \boldsymbol{r}_1} + \frac{\boldsymbol{F}_{ext}+\boldsymbol{F}_{att}}{m}\cdot\frac{\partial f^{(1)}}{\partial \boldsymbol{\xi}_1} \\
&\qquad = -\frac{1}{\tau}\left[f^{(2)} - f^{eq}(1-\mathrm{Pr})\frac{\boldsymbol{c}\cdot\boldsymbol{Q}_k^{(2)}}{5p_0RT}\left(\frac{c^2}{RT}-5\right)\right] + \mathcal{I}^{(2)}.
\end{aligned} \tag{A 2}$$

From the result on the order $\varepsilon^{(0)}$, we can get that

$$\int \Psi_i f^k \mathrm{d}\boldsymbol{\xi} = 0, \quad k \geqslant 1, \tag{A 3}$$

where $\Psi_i = \{1, m\boldsymbol{\xi}, m\boldsymbol{\xi}^2/2\}$ is the summation invariants. Consequently, the hydrodynamic equations at the order of $\varepsilon^{(1)}$ can be obtained as

$$\begin{aligned}
\frac{\partial \rho}{\partial t_1} + \frac{\partial}{\partial \boldsymbol{r}_1}\cdot(\rho\boldsymbol{u}) = 0, \\
\frac{\partial(\rho\boldsymbol{u})}{\partial t_1} + \frac{\partial}{\partial \boldsymbol{r}_1}\cdot[\boldsymbol{P}_k^{(0)} + \rho\boldsymbol{u}\boldsymbol{u}] - n(\boldsymbol{F}_{ext}+\boldsymbol{F}_{att}) = -\nabla(nV_0\chi nk_BT), \\
\frac{\partial(\rho E)}{\partial t_1} + \frac{\partial}{\partial \boldsymbol{r}_1}\cdot[\boldsymbol{Q}_k^{(0)} + \rho E\boldsymbol{u} + \boldsymbol{P}_k^{(0)}\cdot\boldsymbol{u}] - n(\boldsymbol{F}_{ext}+\boldsymbol{F}_{att})\cdot\boldsymbol{u} \\
= -(nV_0\chi nk_BT)(\nabla\cdot\boldsymbol{u}),
\end{aligned} \tag{A 4}$$

where $E = (\boldsymbol{u}^2 + 3RT)/2$ is the total energy per unit mass of gases, and the zeroth order pressure tensor $\boldsymbol{P}_k^{(0)}$ and heat flux $\boldsymbol{Q}_k^{(0)}$ can be calculated as

$$\begin{aligned}
\boldsymbol{P}_k^{(0)} &= \int m\boldsymbol{c}\boldsymbol{c} f^{(0)}\mathrm{d}\boldsymbol{\xi} = nk_BT\boldsymbol{U}, \\
\boldsymbol{Q}_{\boldsymbol{k}}{}^{(0)} &= \int \frac{mc^2\boldsymbol{c}}{2} f^{(0)}\mathrm{d}\boldsymbol{\xi} = 0,
\end{aligned} \tag{A 5}$$

where $\boldsymbol{U}$ is the unit tensor.

Similarly, the hydrodynamic equations on the order of $\varepsilon^{(2)}$ can be obtained by taking the moments in terms of the summation invariants Ψ_i as

$$\begin{aligned}
\frac{\partial \rho}{\partial t_2} = 0, \\
\frac{\partial(\rho\boldsymbol{u})}{\partial t_2} + \frac{\partial}{\partial \boldsymbol{r}_1}\cdot\boldsymbol{P}_{\boldsymbol{k}}{}^{(1)} = \nabla[\mu_B(\nabla\cdot\boldsymbol{u})], \\
\frac{\partial(\rho E)}{\partial t_2} + \frac{\partial}{\partial \boldsymbol{r}_1}\cdot[\boldsymbol{Q}_k^{(1)} + \boldsymbol{P}_k^{(1)}\cdot\boldsymbol{u}] = \mu_B(\nabla\cdot\boldsymbol{u})^2,
\end{aligned} \tag{A 6}$$

where the first order pressure tensor $\boldsymbol{P}_k^{(1)}$ and heat flux $\boldsymbol{Q}_k^{(1)}$ can be calculated as

$$\begin{aligned}\boldsymbol{P}_k^{(1)} &= \int m\boldsymbol{c}\boldsymbol{c} f^{(1)} \mathrm{d}\boldsymbol{\xi} = -2nk_B T\tau \left(1 + \frac{2}{5}nV_0\chi\right) \mathring{\boldsymbol{S}}, \\ \boldsymbol{Q}_k^{(1)} &= \int \frac{mc^2\boldsymbol{c}}{2} f^{(1)} \mathrm{d}\boldsymbol{\xi} = -\frac{5k_B}{2m}\frac{nk_B T\tau}{\mathrm{Pr}} \left(1 + \frac{3}{5}nV_0\chi\right) \nabla T,\end{aligned} \tag{A 7}$$

where $f^{(1)}$ can be obtained from the $\varepsilon^{(1)}$ order relationship in equation (A 2) as

$$\begin{aligned} f^{(1)} = -\tau &\left[\frac{\partial f^{(0)}}{\partial t_1} + \boldsymbol{\xi}\cdot\frac{\partial f^{(0)}}{\partial \boldsymbol{r}_1} + \frac{\boldsymbol{F}_{ext} + \boldsymbol{F}_{att}}{m}\cdot\frac{\partial f^{(0)}}{\partial \boldsymbol{\xi}_1}\right] \\ &+ f^{eq}(1-\mathrm{Pr})\frac{\boldsymbol{c}\cdot\boldsymbol{Q}_k^{(1)}}{5p_0RT}\left(\frac{c^2}{RT} - 5\right) + \tau\mathcal{I}^{(1)},\end{aligned} \tag{A 8}$$

and $\mathring{\boldsymbol{S}}$ is the rate-of-shear tensor expressed as

$$\mathring{\boldsymbol{S}} = \frac{1}{2}\left[\nabla\boldsymbol{u} + (\nabla\boldsymbol{u})^{\top}\right] - \frac{1}{3}(\nabla\cdot\boldsymbol{u})\boldsymbol{U}, \tag{A 9}$$

where $(\nabla\boldsymbol{u})^{\top}$ denotes the transpose of $\nabla\boldsymbol{u}$.

If the size of the gas molecule is not negligible, the momentum and energy can be transferred at the instant collisions over a molecule size σ. According to Cercignani & Lampis (1988) and Frezzotti (1999), the collisional pressure tensor $\boldsymbol{P}_c$ and heat flux $\boldsymbol{Q}_c$ relate to the collision operator through

$$\begin{aligned}\int m\boldsymbol{\xi}[J_s^{(0)} + \mathcal{I}^{(1)} + \mathcal{I}^{(2)}]\mathrm{d}\boldsymbol{\xi} &= -\nabla\cdot\boldsymbol{P}_c, \\ \int \frac{m\xi^2}{2}[J_s^{(0)} + \mathcal{I}^{(1)} + \mathcal{I}^{(2)}]\mathrm{d}\boldsymbol{\xi} &= -\nabla\cdot(\boldsymbol{Q}_c + \boldsymbol{P}_c\cdot\boldsymbol{u}),\end{aligned} \tag{A 10}$$

from which we can get

$$\begin{aligned}\boldsymbol{P}_c &= [nk_B TnV_0\chi - \mu_B(\nabla\cdot\boldsymbol{u})]\boldsymbol{U}, \\ \boldsymbol{Q}_c &= 0.\end{aligned} \tag{A 11}$$

The total pressure tensor $\boldsymbol{P}$ and heat flux $\boldsymbol{Q}$ are the combination of kinetic and collisional contributions, which are

$$\begin{aligned}\boldsymbol{P} &= [nk_B TnV_0\chi - \mu_B(\nabla\cdot\boldsymbol{u})]\boldsymbol{U} - 2nk_B T\tau\left(1 + \frac{2}{5}nV_0\chi\right)\mathring{\boldsymbol{S}}, \\ \boldsymbol{Q} &= -\frac{5k_B}{2m}\frac{nk_B T\tau}{\mathrm{Pr}}\left(1 + \frac{3}{5}nV_0\chi\right)\nabla T.\end{aligned} \tag{A 12}$$

Comparing (A 12) to the Newton's law of viscosity and the Fourier's law of thermal conduction, the relationship between the relaxation time and transport coefficients can be obtained as

$$\begin{aligned}\mu_s &= nk_B T\tau\left(1 + \frac{2}{5}nV_0\chi\right), \\ \kappa &= \frac{5k_B}{2m}\frac{nk_B T\tau}{\mathrm{Pr}}\left(1 + \frac{3}{5}nV_0\chi\right).\end{aligned} \tag{A 13}$$

When the long-range attraction between gas molecules is considered, the intermolecular potential energy comes into play (Chapman & Cowling 1990; Martys 1999; He & Doolen

2002). Assuming that the density varies slowly with space in the hydrodynamic limit, the mean-field force term can be approximated by

$$\boldsymbol{F}_{att} = 2a\nabla n + k\nabla\nabla^2 n, \tag{A 14}$$

where a and k are two constants related to the attractive potential as

$$\begin{aligned} a &= -\frac{1}{2}\int_{r>\sigma} \phi_{att}(r)\mathrm{d}\boldsymbol{r}, \\ k &= -\frac{1}{6}\int_{r>\sigma} r^2\phi_{att}(r)\mathrm{d}\boldsymbol{r}. \end{aligned} \tag{A 15}$$

Considering the identity of $n\nabla\nabla^2 n$ in the form of

$$n\nabla\nabla^2 n = \nabla\cdot\left[\left(n\nabla^2 n + \frac{1}{2}|\nabla n|^2\right)\boldsymbol{U} - \nabla n\nabla n\right], \tag{A 16}$$

the mean-field force term in (A 4) can be transformed as

$$n\boldsymbol{F}_{att} = a\nabla n^2 + k\nabla\cdot\left[\left(n\nabla^2 n + \frac{1}{2}|\nabla n|^2\right)\boldsymbol{U} - \nabla n\nabla n\right]. \tag{A 17}$$

Finally, combining (A 4), (A 6) and (A 17), we obtain the hydrodynamic equations of the kinetic model (2.16) in the following form

$$\begin{aligned} \frac{\partial\rho}{\partial t} + \nabla\cdot(\rho\boldsymbol{u}) &= 0, \\ \frac{\partial(\rho\boldsymbol{u})}{\partial t} + \nabla\cdot(\rho\boldsymbol{u}\boldsymbol{u}) + \nabla[p - \mu_B(\nabla\cdot\boldsymbol{u})] - \nabla\cdot(2\mu_s\mathring{\boldsymbol{S}}) - \nabla\cdot\boldsymbol{K} - n\boldsymbol{F}_{ext} &= 0, \\ \frac{\partial(\rho E)}{\partial t} + \nabla\cdot(\rho E\boldsymbol{u}) - \nabla\cdot(\kappa\nabla T) + [p - \mu_B(\nabla\cdot\boldsymbol{u})](\nabla\cdot\boldsymbol{u}) - (2\mu_s\mathring{\boldsymbol{S}}) : \nabla\boldsymbol{u} & \\ -\boldsymbol{K} : \nabla\boldsymbol{u} - n\boldsymbol{F}_{ext}\cdot\boldsymbol{u} &= 0, \end{aligned} \tag{A 18}$$

where the pressure p in both the momentum and energy equations satisfies

$$p = nk_B T(1 + nV_0\chi) - an^2, \tag{A 19}$$

and $\boldsymbol{K}$ is the capillary tensor given by

$$\boldsymbol{K} = k\left[\left(n\nabla^2 n + \frac{1}{2}|\nabla n|^2\right)\boldsymbol{U} - \nabla n\nabla n\right]. \tag{A 20}$$

Noted that if there is no interface, e.g. for single phase flows, the capillary force does not appear, and the hydrodynamic equations (A 18) reduce to the conventional NS equations for compressible flows.

REFERENCES

Alexander, Francis J, Garcia, Alejandro L & Alder, Berni J 1995 A consistent boltzmann algorithm. *Phys. Rev. Lett.* **74** (26), 5212.

Amorós, J, Maeso, MJ & Villar, E 1992 A test of the modified enskog theory for the transport properties of liquids. *Int. J. Thermophys.* **13** (5), 907–920.

Andersen, Hans C, Weeks, John D & Chandler, David 1971 Relationship between the hard-sphere fluid and fluids with realistic repulsive forces. *Phys. Rev. A* **4** (4), 1597.

Barker, John A & Henderson, Douglas 1967 Perturbation theory and equation of state for fluids. ii. a successful theory of liquids. *J. Chem. Phys.* **47** (11), 4714–4721.

van Beijeren, Henk 1983 Equilibrium distribution of hard-sphere systems and revised enskog theory. *Phys. Rev. Lett.* **51** (17), 1503.

van Beijeren, Henk & Ernst, Matthieu H 1973 The modified enskog equation. *Physica* **68** (3), 437–456.

Ben-Amotz, Dor & Herschbach, Dudley R 1990 Estimation of effective diameters for molecular fluids. *J. Phys. Chem.* **94** (3), 1038–1047.

Borgelt, P, Hoheisel, C & Stell, G 1990 Exact molecular dynamics and kinetic theory results for thermal transport coefficients of the lennard-jones argon fluid in a wide region of states. *Phys. Rev. A* **42** (2), 789.

Carnahan, Norman F & Starling, Kenneth E 1969 Equation of state for nonattracting rigid spheres. *J. Chem. Phys.* **51** (2), 635–636.

Cercignani, Carlo & Lampis, Maria 1988 Kinetic theory of a dense gas of rough spheres. *J. Stat. Phys.* **53**.

Chapman, Sydney & Cowling, Thomas George 1990 *The mathematical theory of non-uniform gases: an account of the kinetic theory of viscosity, thermal conduction and diffusion in gases*. Cambridge university press.

Chatwell, René Spencer & Vrabec, Jadran 2020 Bulk viscosity of liquid noble gases. *J. Chem. Phys.* **152** (9), 094503.

Chung, Ting Horng, Ajlan, Mohammad, Lee, Lloyd L & Starling, Kenneth E 1988 Generalized multiparameter correlation for nonpolar and polar fluid transport properties. *Ind. Eng. Chem. Res.* **27** (4), 671–679.

Chung, Ting Horng, Lee, Lloyd L & Starling, Kenneth E 1984 Applications of kinetic gas theories and multiparameter correlation for prediction of dilute gas viscosity and thermal conductivity. *Ind. Eng. Chem. Fundam.* **23** (1), 8–13.

Collings, AF & Hain, DL 1976 The density dependence of bulk viscosity in a simple dense gas. *J. Chem. Phys.* **65** (8), 2995–2997.

Corral-Casas, Carlos, Li, Jun, Borg, Matthew K & Gibelli, Livio 2022 Knudsen minimum disappearance in molecular-confined flows. *J. Fluid Mech.* **945**, A28.

Cotterman, RL, Schwarz, BJ & Prausnitz, JM 1986 Molecular thermodynamics for fluids at low and high densities. part i: Pure fluids containing small or large molecules. *AICHE J.* **32** (11), 1787–1798.

Enskog, D 1921 The numerical calculation of phenomena in fairly dense gases. *Arkiv Mat. Astr. Fys* **16** (1), 1–60.

Ferziger, Joel H & Kaper, Hans G 1972 *Mathematical theory of transport processes in gases*. North-Holland Publishing Company.

Frezzotti, Aldo 1997 Molecular dynamics and enskog theory calculation of one dimensional problems in the dynamics of dense gases. *Physica A* **240** (1-2), 202–211.

Frezzotti, Aldo 1999 Monte carlo simulation of the heat flow in a dense hard sphere gas. *Eur. J. Mech. B-Fluid* **18** (1), 103–119.

Frezzotti, A, Barbante, Paolo & Gibelli, Livio 2019 Direct simulation monte carlo applications to liquid-vapor flows. *Phys. Fluids* **31** (6), 062103.

Frezzotti, Aldo & Sgarra, Carlo 1993 Numerical analysis of a shock-wave solution of the enskog equation obtained via a monte carlo method. *J. Stat. Phys.* **73** (1), 193–207.

Gan, Yanbiao, Xu, Aiguo, Lai, Huilin, Li, Wei, Sun, Guanglan & Succi, Sauro 2022 Discrete boltzmann multi-scale modeling of non-equilibrium multiphase flows. *J. Fluid Mech.* **951**, A8.

Gray, Peter & Rice, Stuart A 1964 On the kinetic theory of dense fluids. xviii. the bulk viscosity. *J. Chem. Phys.* **41** (12), 3689–3694.

Guo, Zhaoli & Shu, Chang 2013 *Lattice Boltzmann method and its application in engineering*, , vol. 3. World Scientific.

Guo, Zhaoli, Zhao, TS & Shi, Yong 2005 Simple kinetic model for fluid flows in the nanometer scale. *Phys. Rev. E* **71** (3), 035301.

Guo, Zhaoli, Zhao, TS & Shi, Yong 2006 Generalized hydrodynamic model for fluid flows: From nanoscale to macroscale. *Phys. Fluids* **18** (6), 067107.

Hanley, HJM, McCarty, RD & Cohen, EGD 1972 Analysis of the transport coefficients for simple dense fluid: Application of the modified enskog theory. *Physica* **60** (2), 322–356.

Haynes, WM 1973 Viscosity of gaseous and liquid argon. *Physica* **67** (3), 440–470.

He, Xiaoyi & Doolen, Gary D 2002 Thermodynamic foundations of kinetic theory and lattice boltzmann models for multiphase flows. *J. Stat. Phys.* **107** (1), 309–328.

He, Xiaoyi, Shan, Xiaowen & Doolen, Gary D 1998 Discrete boltzmann equation model for nonideal gases. *Phys. Rev. E* **57** (1), R13.

Hoover, William G, Evans, Denis J, Hickman, Richard B, Ladd, Anthony JC, Ashurst, William T & Moran, Bill 1980*a* Lennard-jones triple-point bulk and shear viscosities. green-kubo theory, hamiltonian mechanics, and nonequilibrium molecular dynamics. *Phys. Rev. A* **22** (4), 1690.

Hoover, William G, Ladd, Anthony JC, Hickman, Richard B & Holian, Brad Lee 1980*b* Bulk viscosity via nonequilibrium and equilibrium molecular dynamics. *Phys. Rev. A* **21** (5), 1756.

Huang, Rongzong, Li, Qing & Adams, Nikolaus A 2022 Surface thermodynamics and wetting condition in the multiphase lattice boltzmann model with self-tuning equation of state. *J. Fluid Mech.* **940**.

Huang, Rongzong, Wu, Huiying & Adams, Nikolaus A 2021 Mesoscopic lattice boltzmann modeling of the liquid-vapor phase transition. *Phys. Rev. Lett.* **126** (24), 244501.

Jaeger, Frederike, Matar, Omar K & Müller, Erich A 2018 Bulk viscosity of molecular fluids. *J. Chem. Phys.* **148** (17), 174504.

Joseph, Sony & Aluru, NR 2008 Why are carbon nanotubes fast transporters of water? *Nano Lett.* **8** (2), 452–458.

Karkheck, John & Stell, George 1981 Kinetic mean-field theories. *J. Chem. Phys.* **75** (3), 1475–1487.

Kogan, MN 1973 Molecular gas dynamics. *Annu. Rev. Fluid Mech.* **5** (1), 383–404.

Kremer, Gilberto M 2010 *An introduction to the Boltzmann equation and transport processes in gases*. Springer Science & Business Media.

Luo, Lishi 2000 Theory of the lattice boltzmann method: Lattice boltzmann models for nonideal gases. *Phys. Rev. E* **62** (4), 4982.

Luo, Li-Shi 1998 Unified theory of lattice boltzmann models for nonideal gases. *Phys. Rev. Lett.* **81** (8), 1618.

Madigosky, WM 1967 Density dependence of the bulk viscosity in argon. *J. Chem. Phys.* **46** (11), 4441–4444.

Malbrunot, P, Boyer, A, Charles, E & Abachi, H 1983 Experimental bulk viscosities of argon, krypton, and xenon near their triple point. *Phys. Rev. A* **27** (3), 1523.

Martini, Ashlie, Hsu, Hua-Yi, Patankar, Neelesh A & Lichter, Seth 2008 Slip at high shear rates. *Phys. Rev. Lett.* **100** (20), 206001.

Martys, Nicos S 1999 Energy conserving discrete boltzmann equation for nonideal systems. *Int. J. Mod. Phys. C* **10** (07), 1367–1382.

Maxwell, J Clerk 1874 Van der waals on the continuity of the gaseous and liquid states. *Nature* **10** (259), 477–480.

Mehrabi, Mehran, Javadpour, Farzam & Sepehrnoori, Kamy 2017 Analytical analysis of gas diffusion into non-circular pores of shale organic matter. *J. Fluid Mech.* **819**, 656–677.

Michels, A, Sengers, JV & Van de Klundert, LJM 1963 The thermal conductivity of argon at elevated densities. *Physica* **29** (2), 149–160.

Neufeld, Philip D, Janzen, AR & Aziz, R_A 1972 Empirical equations to calculate 16 of the transport collision integrals ω (l, s)* for the lennard-jones (12–6) potential. *J. Chem. Phys.* **57** (3), 1100–1102.

Nie, XB, Chen, SY, Robbins, MarkO & others 2004 A continuum and molecular dynamics hybrid method for micro-and nano-fluid flow. *J. Fluid Mech.* **500**, 55–64.

Rana, Anirudh S, Lockerby, Duncan A & Sprittles, James E 2018 Evaporation-driven vapour microflows: analytical solutions from moment methods. *J. Fluid Mech.* **841**, 962–988.

Rangel-Huerta, A & Velasco, RM 1996 Generalized bulk viscosity for enskog gases. *J. Non-Equilib. Thermodyn.* .

Reichl, LE 1998 *A modern course in statistical physics*. Wiley, New.

Restrepo, Julián & Simões-Moreira, José R 2022 Viscous effects on real gases in quasi-one-dimensional supersonic convergent divergent nozzle flows. *J. Fluid Mech.* **951**, A14.

Sadr, Mohsen & Gorji, M Hossein 2017 A continuous stochastic model for non-equilibrium dense gases. *Phys. Fluids* **29** (12), 122007.

Sadr, Mohsen & Gorji, M Hossein 2019 Treatment of long-range interactions arising in the enskog–vlasov description of dense fluids. *J. Comput. Phys.* **378**, 129–142.

Sadr, Mohsen, Pfeiffer, Marcel & Gorji, M Hossein 2021 Fokker-planck-poisson kinetics: multi-phase flow beyond equilibrium. *J. Fluid Mech.* **920**.

Shakhov, EM 1968 Generalization of the krook kinetic relaxation equation. *Fluid Dynam+* **3** (5), 95–96.

Shan, Baochao, Wang, Peng, Zhang, Yonghao & Guo, Zhaoli 2020 Discrete unified gas kinetic scheme for all knudsen number flows. iv. strongly inhomogeneous fluids. *Phys. Rev. E* **101** (4), 043303.

Shan, Baochao, Wang, Runxi, Guo, Zhaoli & Wang, Peng 2021 Contribution quantification of nanoscale gas transport in shale based on strongly inhomogeneous kinetic model. *Energy* **228**, 120545.

Sheng, Qiang, Gibelli, Livio, Li, Jun, Borg, Matthew K & Zhang, Yonghao 2020 Dense gas flow simulations in ultra-tight confinement. *Phys. Fluids* **32** (9), 092003.

Sobrino, Luis de 1967 On the kinetic theory of a van der waals gas. *Can. J. Phys.* **45** (2), 363–385.

Su, Wei, Gibelli, Livio, Li, Jun, Borg, Matthew K. & Zhang, Yonghao 2023 Kinetic modeling of nonequilibrium flow of hard-sphere dense gases. *Phys. Rev. Fluids* **8**, 013401.

Su, Wei, Wang, Peng, Zhang, Yonghao & Wu, Lei 2020 Implicit discontinuous galerkin method for the boltzmann equation. *Journal of Scientific Computing* **82**, 1–35.

Suryanarayanan, Saikishan, Singh, Shiwani & Ansumali, Santosh 2013 Extended bgk boltzmann for dense gases. *Commun. Comput. Phys.* **13** (3), 629–648.

Takata, Shigeru, Matsumoto, Takuya & Hattori, Masanari 2021 Kinetic model for the phase transition of the van der waals fluid. *Phys. Rev. E* **103** (6), 062110.

Takata, Shigeru & Noguchi, Takashi 2018 A simple kinetic model for the phase transition of the van der waals fluid. *J. Stat. Phys.* **172** (3), 880–903.

Tarazona, Pedro 1985 Free-energy density functional for hard spheres. *Phys. Rev. A* **31** (4), 2672.

Todd, Billy D 2001 Computer simulation of simple and complex atomistic fluids by nonequilibrium molecular dynamics techniques. *Comput. Phys. Commun.* **142** (1-3), 14–21.

Torres-Herrera, Ulises & Poiré, Eugenia Corvera 2021 A continuum model to study fluid dynamics within oscillating elastic nanotubes. *J. Fluid Mech.* **916**.

Torrilhon, Manuel 2016 Modeling nonequilibrium gas flow based on moment equations. *Annu. Rev. Fluid Mech.* **48**, 429–458.

Van Erp, Remco, Soleimanzadeh, Reza, Nela, Luca, Kampitsis, Georgios & Matioli, Elison 2020 Co-designing electronics with microfluidics for more sustainable cooling. *Nature* **585** (7824), 211–216.

Vera, JH & Prausnitz, JM 1972 Generalized van der waals theory for dense fluids. *Chem. Eng. J.* **3**, 1–13.

van der Waals, Johannes Diderik 1873 *Over de Continuiteit van den Gas-en Vloeistoftoestand*, , vol. 1. Sijthoff.

Wang, Moran & Li, Zhixin 2007 An enskog based monte carlo method for high knudsen number non-ideal gas flows. *Comput. Fluids* **36** (8), 1291–1297.

Wang, Peng, Wu, Lei, Ho, Minh Tuan, Li, Jun, Li, Zhi-Hui & Zhang, Yonghao 2020 The kinetic shakhov–enskog model for non-equilibrium flow of dense gases. *J. Fluid Mech.* **883**.

Wang, Ziyan, Wang, Moran & Chen, Shiyi 2018 Coupling of high knudsen number and non-ideal gas effects in microporous media. *J. Fluid Mech.* **840**, 56–73.

Wu, Lei, Liu, Haihu, Reese, Jason M & Zhang, Yonghao 2016 Non-equilibrium dynamics of dense gas under tight confinement. *J. Fluid Mech.* **794**, 252–266.

Wu, Lei, Zhang, Yonghao & Reese, Jason M 2015 Fast spectral solution of the generalized enskog equation for dense gases. *J. Comput. Phys.* **303**, 66–79.

Zhang, Liehui, Shan, Baochao, Zhao, Yulong & Guo, Zhaoli 2019 Review of micro seepage mechanisms in shale gas reservoirs. *Int. J. Heat Mass Tran.* **139**, 144–179.

Zhao, Yulong, Zhang, Liehui, Luo, Jianxin & Zhang, Boning 2014 Performance of fractured horizontal well with stimulated reservoir volume in unconventional gas reservoir. *J. Hydrol.* **512**, 447–456.